frontiers in Marine Science

ORIGINAL RESEARCH
published: 17 November 2021
doi: 10.3389/fmars.2021.671362

Differences in the Structural Components Influence the Pumping Capacity of Marine Sponges

Azraj S. Dahihande[1,2†] *and Narsinh L. Thakur*[1*†]

[1] *Academy of Scientific and Innovative Research (AcSIR), Department of Chemical Oceanography, CSIR-National Institute of Oceanography, Goa, India,* [2] *Maratha Vidya Prasarak Samaj, Karmveer Abasaheb Alias N. M. Sonawane Arts, Commerce, and Science College, Nashik, India*

OPEN ACCESS

Edited by:
Neloy Khare,
Ministry of Earth Sciences, India

Reviewed by:
Anja Schulze,
Texas A&M University at Galveston, United States
Christopher J. Freeman,
College of Charleston, United States

***Correspondence:**
Narsinh L. Thakur
thakurn@nio.org

[†] *These authors have contributed equally to this work*

Specialty section:
This article was submitted to Marine Evolutionary Biology, Biogeography and Species Diversity, a section of the journal Frontiers in Marine Science

Received: *23 February 2021*
Accepted: *17 September 2021*
Published: *17 November 2021*

Citation:
Dahihande AS and Thakur NL (2021) Differences in the Structural Components Influence the Pumping Capacity of Marine Sponges. Front. Mar. Sci. 8:671362. doi: 10.3389/fmars.2021.671362

Marine sponges are important sessile, benthic filter feeders with a body plan designed to pump water efficiently. The sponge body plan generally consists of mineral spicules, gelatinous mesohyl, and the pores and canals of the aquiferous system. These structural components have stark differences in compressibility, mass, and volume; therefore, their proportion and distribution are likely to affect sponge morphology, anatomy, contraction, and finally the pumping capacity. We examined seven demosponge species (from high spicule skeleton contents to no spicules) commonly found along the central west coast of India for structural components, such as total inorganic contents (spicule skeleton and foreign inclusions), body density, porosity, and mesohyl TEM for the high microbial abundance/low microbial abundance status. Additionally, we estimated the sponge pumping rate by measuring the excurrent velocity, the abundance of individual pumping units and cells, i.e., choanocyte chambers and choanocytes, and also carried out a morphometric analysis of aquiferous structures. The excurrent velocity and the oscular flow rates showed a positive relationship with the oscular crosssectional area for all the study species. The inorganic spicule contents by their weight as well as volume formed a major component of tissue density and higher proportions of spicules were associated with reduced aquiferous structures and lower pumping rate. The ash mass% and the ash free dry weight (AFDW %) in the sponge dry mass showed separate and distinct associations with aquiferous system variables. For example, the number of choanocytes per chamber showed a wide difference between the studied species ranging from 35.02 ± 2.44 (*C.* cf. *cavernosa*) to 120.35 ± 8.98 (*I. fusca*) and had a significant positive relationship with AFDW% and a negative relationship with ash mass%. This study indicates that the differences in the proportions of structural components are closely related to sponge gross morphology, anatomy, and probably body contractions, factors that influence the sponge pumping capacity.

Keywords: pumping, spicules, sponge (porifera), mesohyl, choanocyte chamber, aquiferous module, canal

INTRODUCTION

Poriferans (sponges) are found in almost all benthic habitats and are capable of processing the volume of water several times their body volume per hour (Reiswig, 1971, 1981; Riisgaard and Larsen, 1995). Filter feeding sponges play an important role in recycling nutrients and coupling pelagic food supply with benthic communities (Gili J M Coma, 1998; Maldonado et al., 2012; Pawlik and McMurray, 2020). Although, being filter feeders, a major portion of sponge diet is composed of the dissolved organic carbon (DOC) (Yahel et al., 2003; McMurray et al., 2016) and it is suggested that sponge assimilated DOC facilitates its bioavailability to other tropic levels in form of detritus (De Goeij et al., 2013) and biomass that feeds various sponge predators (McMurray et al., 2018).

Considering the wide distribution range and exposure to different environmental regimes, different morphological adaptations are observed in sponges. These morphological differences can manifest on macro as well as microlevels i.e., gross morphology and spicule morphology, respectively (Bell et al., 2002). Sponges are sessile metazoans lacking muscular, nervous, and digestive systems. Instead, they have a body full of pores and canals with a body plan designed to efficiently pump water. The sponge body plan generally consists of three major structural features, the aquiferous system, gelatinous mesohyl, and the spicule skeleton. The aquiferous system constitutes the pores, canals, and hollow spaces that conduct a unidirectional flow of water to filter and absorb the nutrients, exchange gases, and expel the waste products. The mesohyl is a gelatinous matrix with a free-floating population of different cell types and is bound between choanoderm and pinacoderm made of flagellated choanocytes and flattened pinacocytes, respectively. The pinacoderm covering the outer surface of the sponge is referred to as an exopinacoderm and the layer of pinacocytes lining the canals inside the sponge is referred to as endopinacoderm (Leys and Hill, 2012). The spicule skeleton consists of microscopic inorganic spicules. The mesohyl and the spicule skeleton support the pores and the canals of the aquiferous system by forming a three-dimensional scaffold structure.

Scaffold design is an important aspect of tissue engineering, and studies show that successful designs require a fine balance between mechanical function and interconnected pore network for flow transport of nutrients and metabolic waste (Hollister et al., 2000; Hutmacher, 2000; Hollister, 2005). This balance is often achieved by a trade-off mechanism between a denser scaffold for better mechanical function and a more porous scaffold for better flow transport (Hollister, 2005). Such mechanisms are evident in sponges. The proportion and distribution of scaffold materials (spicule skeleton and mesohyl), and the pore network (aquiferous system) have variations within and between species as a function of ecology and natural history. For instance, sponges have narrower canals when the proportion of spicules is higher in high disturbance environments (Palumbi, 1986) or when the mesohyl is densely packed with high biomass of associated microbes (Vacelet and Donadey, 1977; Wilkinson, 1978, 1983). Sponges have evolved strong symbiotic association with microorganisms (Taylor et al., 2007) and are characterized into two distinct categories of high microbial abundance (HMA) sponges and low microbial abundance (LMA) sponges based on the abundance of microbes within the mesohyl (Hentsshel et al., 2003). Both HMA and LMA sponges show a high degree of host specificity and temporal stability of the microbial symbionts with low seasonal and interannual variation (Taylor et al., 2007; Gloeckner et al., 2014; Erwin et al., 2015). In HMA sponges, the mesohyl with the microbial biomass can comprise up to one-third of the total sponge biomass (Vacelet and Donadey, 1977). When compared with LMA sponges, the disproportionate increase in the mesohyl of HMA sponges is associated with an increase in tissue density (Weisz et al., 2008), a decrease in the abundance of choanocyte chambers (CC; Poppell et al., 2014), and the narrowing of canal (Vacelet and Donadey, 1977) features that are related to the aquiferous system.

Although sponges have high anatomical and morphological variation, the aquiferous system follows specific design principles to control the water velocity at specific regions within the sponge (LaBarbera and Vogel, 1982; LaBarbera, 1990; Labarbera, 1995; Vogel, 1996). This has a functional significance and is evident in the morphometric models which show that the canal systems of sponges with different morphologies reduce water velocities at the filtering structures to enable nutrition absorption and food capture (Leys et al., 2011; Ludeman et al., 2016). The water flow in the aquiferous system starts at the numerous microscopic inhalant pores called ostia, present on the external body surface. Beneath the ostia are subdermal lacunar spaces connected to the incurrent canals that successively branch into fine, narrower canals and open into the CC *via* a pore called a porospyle. The CC is lined with cells that have an apical flagellum, surrounded by a microvillar collar. Here, the incurrent water spreads and slows down due to the increased surface area of the numerous narrow canals and the microvillar collar. This helps to filter and absorb the particles and exchange the gases. The filtered water flows out of the CC into the excurrent canals *via* a pore called apopyle. The increasing diameter and the reducing surface area of the converging excurrent canals expel the water out of the osculum, the excurrent opening, with a high velocity so that same water is not refiltered (Riisgård et al., 1993; Riisgaard and Larsen, 1995; Leys et al., 2011; Ludeman et al., 2016).

The efficacy of the aquiferous system would depend on the canal architecture with optimum branching pattern. However, high-resolution 3D reconstructions of the aquiferous system of sponge *Tethya wilhelma* show that the aquiferous system architecture diverges from the theoretical optimum and the branching topology follows a non-hierarchical and a non-uniform pattern (Hammel et al., 2012). This deviation could be attributed to the interdependent development of the canal structures, skeletal structures, and sponge tissue (Hammel et al., 2012). For example, morphologically similar sponges *Haliclona permollis* and *Halicondria panacea* vary in the cross sectional area of ostia due to differences in the spicule arrangement (Reiswig, 1975). Additionally, the erect tree-like growth forms of sponge *Haliclona oculata* and *Haliclona simulans* display radiate-accretive growth, with a regular anisotropic reticulate type of skeleton (de Weerdt, 1986; Kaandorp, 1991), but the

aquiferous system of *H. oculata* is poorly developed, and the canals are only present in proximity to the oscula, whereas in *H. simulans* the aquiferous system is more complex and is visible as an extensive system of canals (de Weerdt, 1986; Kaandorp, 1991). These observations indicate that morphologically similar sponges can differ in their spicule skeleton and show major differences in the architecture of their aquiferous system. These structural components have stark differences in compressibility, mass, and volume; therefore, their proportion and distribution are likely to affect sponge morphology, anatomy, contraction, and pumping capacity.

In the present study, we compare the abundance of the filtration apparatus, dimensions of the aquifereous components, and the pumping parameters in sponges with different proportions of the structural components. To do this, we measured the body density, total inorganic contents (spicule skeleton and foreign inclusions), porosity, and examined the TEM of mesohyl for HMA/LMA status of seven demosponge species (*Cinachyrella* cf. *cavernosa*, *Suberites carnosus*, *Ircinia fusca*, *Amorphinopsis foetida*, *Haliclona* sp., *Calyspongia* sp., and *Biemna fortis*) from the rocky intertidal regions on the west coast of India. We selected sponge species from different sponge taxa representing different characteristics such as psammobiotic species with buried growth form (*B. fortis*) having high inorganic contents and keratose sponges (*Ircinia fusca*) with massive morphology and no mineral spicule skeleton. The species also represented morphological shapes such as tetillid sponge *Cinachyrella* cf. *Cavernosa* having a characteristic spherical morphology with circular depressions called porocalices (Szitenberg et al., 2013) and mineral skeleton of spicule bundles radiating from the sponge center. Other morphological shapes included in the study were the tubular shaped *Haliclona* sp., *Calyspongia* sp., and the thick encrusting form of *A. foetida.* The goal of the present study was to examine the influence of the structural components on sponge pumping by (1) assessing anatomical variations in the sponges with a different morphology from the central west coast of India (2) and determining if structural differences in sponge anatomy influence their function.

MATERIALS AND METHODS

Measurement of Excurrent Velocity and Pumping Rate

The fieldwork was conducted at two intertidal zones, Anjuna (15°33′57.51″N 73° 44′30.39″E) and Kunkeshwar (15°55′28.16″N 73°33′26.69″E) along the Central West Coast of India (**Figure 1**). A total of seven sponge species were included in the present study. The representative specimens of the studied sponges have been deposited at the CSIR–NIO Repository and Taxonomic Center under the following reference code–*A. foetida* (NIO1012/21), *B. fortis* (NIO1011/21), *Calyspongia* sp. (NIO1009/21), *Cinachyrella* cf. *cavernosa* (NIO-41), *Haliclona* sp. (NIO1010/21), *Ircinia fusca* (NIO1007/21), and *Suberites carnosus* (NIO1008/21) (**Figure 1**). Sponge pumping rate was measured using an *in situ* dye technique, as described by Weisz et al. (2008). The volume of water passing through the osculum per second was calculated as a product of excurrent velocity and the osculum crosssectional area. A small volume (2–3 ml) of a concentrated fluorescein dye solution was released near the sponge osculum. The excurrent velocity was determined by video recording the movement of dye fronts. Video recordings were analyzed by monitoring the dye movement frame-by-frame (30 frames per second) with reference to a laminated graph paper held in the background behind the osculum. The travel time of 5–10 dye fronts across the first 3–5 cm was averaged together to obtain the mean excurrent velocity. This mean value was multiplied by the osculum cross sectional area (OSA). Sponge oscula were photographed *in situ*, with an underwater camera and the OSA was measured using functions in ImageJ software. For sponges with more than one osculum, the pumping rate of the whole sponge was obtained by adding the pumping rate measured for each osculum present on that individual. Some of the oscula on multiosculated individuals of *I. fusca* ($n = 6$) and *S. carnosus* ($n = 5$) were not accessible for measurements. In such situations, an average pumping rate (obtained by measuring a minimum of three oscula for each specimen) was used for the osculum that could not be measured. Following the velocity measurements, the whole sponge was collected to measure the sponge biovolume by the water displacement method. It was difficult to determine the individual specimen for *Haliclona* sp., *Calyspongia* sp., and *A. foetida* as the sponges converged and covered large patches of rock ledges or extended inside rock crevices. Therefore, for these sponges, we measured the excurrent velocity on the osculum adjacent to each other and collected that portion of the sponge, and the biovolume was divided by the number of oscula to obtain the biovolume specific pumping rate per osculum. The ratio of volume to dry weight of 3–4 pieces from the collected sponge individuals was calculated to standardize the volume flow rate to dry weight. Before and during all excurrent velocity measurements, no physical contact was made with the sponges.

Structural Components

To measure the body density, tissue composition (organic and inorganic material), and porosity a whole individual (three to nine individuals per species) or a portion of the sponge was fixed in 7% formalin immediately after collection in the field. Sponges were washed in seawater to remove sand and debris from the surface. Sponge volume was determined by measuring the water displacement using the immersion method. The sponge density was measured as the mass (dry weight)/volume ratio. Dry weight (DW) was obtained by drying the samples in an oven at 60°C for more than 48 h (Weisz et al., 2008). To determine the proportion of the spicule skeleton in the body composition, dry sponge samples were combusted in a muffle furnace at 450°C for 8 h (Chanas and Pawlik, 1995). The ash remains i.e., the ash weight (AW) constitute the total inorganic contents (spicule skeleton + foreign inclusion) within the sponge tissue. The proportion of the organic material in the dry bodyweight could be

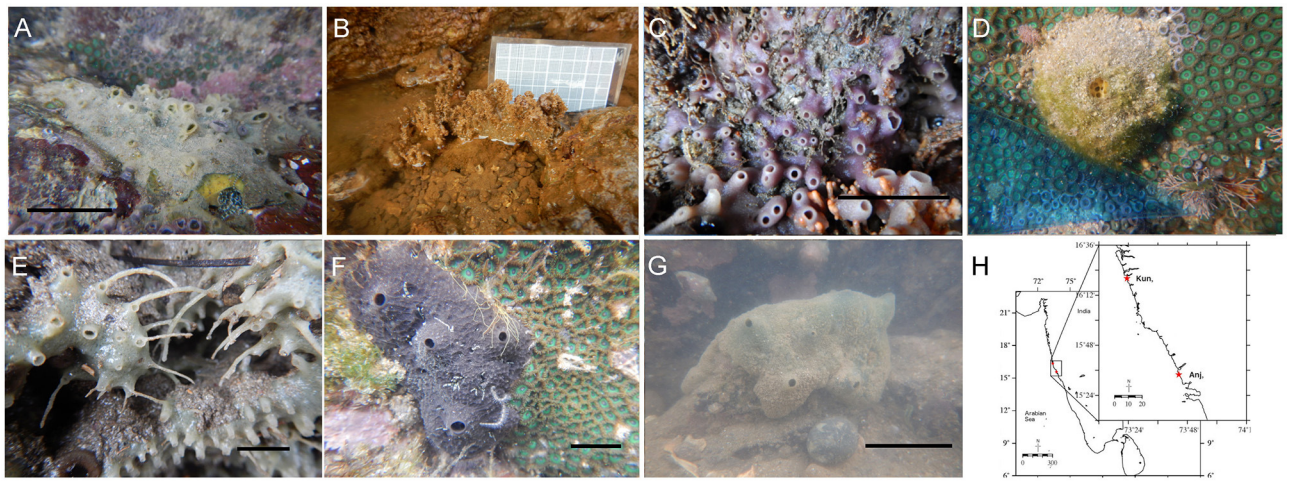

FIGURE 1 | The study species **(A)** *Amorphinopsis foetida,* **(B)** *Biemna fortis,* **(C)** *Calyspongia* sp., **(D)** *Cinachyrella* cf. *cavernosa,* **(E)** *Haliclona* sp., **(F)** *Ircinia fusca,* **(G)** *Suberites carnosus,* **(H)**. The study area showing the location of Anjuna (Anj) and Kunkeshwar (Kun). [Scale **(A)** = 5 cm, **(C)** = 3 cm, **(E)** = 2 cm, **(F)** = 5 cm, **(G)** = 5 cm].

estimated by calculating the ash-free dry weight (AFDW) using the following equation.

$$DW - AW = (AFDW) \quad (1)$$

Since spicules are non-compressible, their volume remains unaltered during body contraction events. Therefore, we also calculated the volumetric proportions of the spicule skeleton and inorganic contents within the sample by dividing the weight data by the material density of substances having comparable density with siliceous spicules (Fang et al., 2013). The material density of opal (2.09 g cm^3) is similar to the siliceous spicules of hexactinellid and demosponge species (Sandford, 2003) and thus was used to calculate the volume proportion of the spicule skeleton within the samples.

The porosity measurements were carried out according to the methods described by Miron-Mendoza et al. (2010). SEM images were subjected to threshold adjustment to convert the pores/canals and collagen/mesohyl matrix to black and white images. The pixel density was adjusted to eliminate the obviously deep collagen fibrils. The 2D black and white representation of the matrix was evaluated using the Analyze Particle Function of ImageJ (particles = black pores).

Morphometric Analysis: Histology and Scanning Electron Microscopy

For morphometric analysis, the dimensions of the aquiferous structures were measured from both histological sections and scanning electron microscopy (SEM) images using ImageJ. For histology, sponge pieces from four to six specimens per species were processed. Samples were fixed in 7% formalin for at least 48 h, rinsed twice in filtered seawater, and then treated with hydrofluoric acid (HF) for 8–10 h to dissolve the spicules. Sponge spicules are frequently dissolved in 5% HF (Langenbruch and Jones, 1990). However, this concentration did not dissolve the spicules completely, so we used 20% HF (Gerasimova and Ereskovsky, 2007) to dissolve the spicules in large sponge pieces, particularly the thick spicule bundles in *C.* cf. *Cavernosa* and the sand grains in the buried growth form of *B. fortis.* The sponge pieces were dehydrated through a graded series of ethanol, embedded in paraffin, sectioned to 5 μm, and stained using Harris's Haematoxylin, and Young's Eosin Erythrosin.

For SEM, two to three sponge pieces (∼10×5 mm) from each species were fixed in a fixative consisting of 2% OsO_4, 2.5% glutaraldehyde in filtered seawater. Some sponge pieces were desilicified in 4% HF then and rinsed with distilled water. Sponge pieces used for porosity measurements were not treated with HF. The samples were dehydrated through a graded series to 100% ethanol, critical point dried (Leica EM CPD300), and then mounted on stubs with double-sided carbon tape. Specimens were then sputter coated in gold: palladium mixture and viewed in a scanning electron microscope. Some pieces of *Ircinia fusca* were embedded in paraffin wax sectioned at 20–30 μm, treated with xylene for 15–20 min to remove the wax, and then processed the same way as other samples.

Mesohyl Examination: Transmission Electron Microscopy

Transmission electron microscopy (TEM) was used to visually assess the bacterial symbionts density in the mesohyl matrix. Freshly collected sponge material of 7–8 mm^3 in size was fixed in 2.5% glutaraldehyde/phosphate-buffered saline for a minimum of 24 h. The samples were rinsed three times for 20 min each in PBS and post-fixed in 2% osmium tetroxide/PBS for 1 h. After fixation, the samples were treated with 5% HF for 2 h to dissolve the spicules followed by three washes in PBS, 20 min each. Samples were dehydrated in ethanol series (30, 50, 70, 90, 3 × 100%), at room temperature and impregnated in the resin. Thin sections were cut with a diamond knife mounted on an

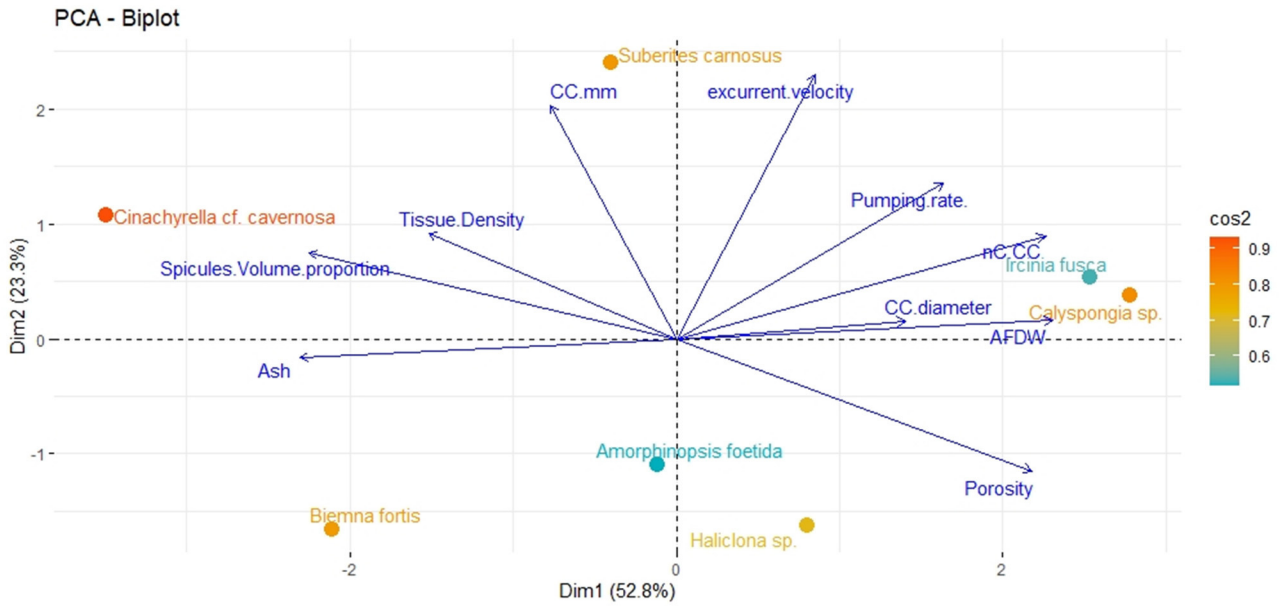

FIGURE 2 | Principal components analysis Dim1 (PCA1) and Dim2 (PCA2) of the combination of structural, filtration, and pumping variables indicating the position of the studied sponge species on a plane defined by the first two axes. Arrows indicate the direction of factor loadings on axes 1 and 2.

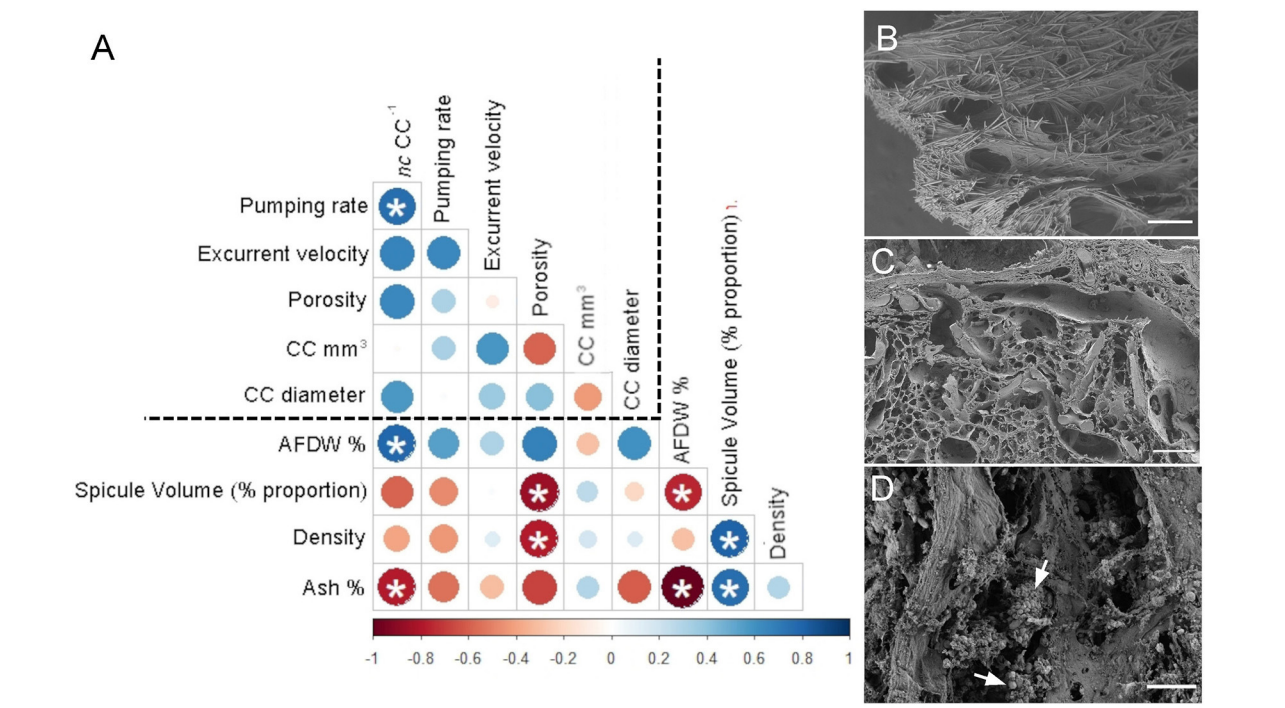

FIGURE 3 | (A) Correlation matrix summarizing all pairwise comparisons between structural components, filtration apparatus, and pumping parameters. The intensity of the color and the size of the circle indicate the strength of the correlation, with red being negative and blue being positive. The dashed line separates the variables related to structural components from the filtration apparatus and pumping parameters. Significant relationships ($p < 0.05$) are marked with an asterix **(B)** *Amorphinopsis feotida* tissue with spicules **(C)** *Ircinia fusca* tissue without any spicules **(D)** *Calyspongia* sp. with the empty spaces around the choanocyte chambers. White arrows point to choanocyte chambers. [scale **(A)** = 500 μm, **(B)** = 100 μm, **(C)** = 20 μm].

ultramicrotome (Cryo-ultra-Microtome, RMC) and stretched on copper grids. The sections were post-stained with uranyl acetate and lead citrate. Micrographs were taken using a Tecnai T12 G2 spirit (FEI) transmission electron microscope.

Data Analysis

An Abundance of Filtration Apparatus (Choanocyte and Choanocyte Chambers)

Six to eight sections per sponge species were photographed at 10X magnification, 10 images per sponge were examined to quantify the number of choanocyte chambers. Repeat count of the CC extending into the adjacent sections was avoided by selecting sections at least 100 μm apart from each other. The number of CC per mm^3 sponge tissue (N) was calculated with the formula used by Abercrombie (1946) with a modification used by Elvin (1976) and Ereskovsky (2000).

$$N = N\left(\frac{t}{D+t}\right)K \tag{2}$$

where N is the average number of CC in the histological section; t is the thickness of the histological section (0.005 mm); D is the diameter of the choanocyte chamber, and K is the constant (200) for converting the number of CC in one square millimeter to the number in a cubic millimeter.

The number of cells along the CC circumference was counted from the SEM images and histological sections to estimate the number of choanocytes per CC with the following formula.

$$ncc = \frac{4\,nc^2}{\pi^2} \tag{3}$$

where *ncc* is the number of choanocytes per CC, *nc* is the count of the choanocytes along the CC circumference.

Multivariate analyses were used to visualize the studied sponge species in multivariate space with respect to the variables related to the structural components, filtration apparatus, and pumping parameters. Multivariate patterns were examined with the principal component analysis (PCA) computed using similarity matrixes based on Euclidean distance on normalized data set as a method of ordination. The loading plots of the PCA analysis indicated potential correlations between the variables (structural components, filtration apparatus, and pumping parameters). Therefore, to examine how the proportions of the structural components affect the variables related to the filtration apparatus and the pumping parameters, we conducted Pearson's correlations. The results were visualized as a correlation matrix using the corrplot package in R (Watson et al., 2017). *B. fortis* did not have excurrent velocity and pumping rate, therefore the data had missing values. To calculate the correlation for every pair of variables without losing information because of missing values, we set the argument to use = "pairwise." To compare the pumping parameters of different sponge species, we explored the relationship of the OSA with the excurrent velocity and the oscular flow rates using ordinary least squares regression. The data were tested for the assumptions of normal distribution, homoscedasticity, and independence of residuals. A multivariate ANOVA (MANOVA) was conducted to compare the variables related to filtration apparatus (CC mm^3, *ncc* CC^{-1}, CC diameter) and structural components (Ash%, AFDW%, porosity%, density, and spicule volume%) as the dependent variables and the sponge species as the independent variables.

RESULTS

Multivariate Analysis and the Relationship Between Structural Components, Filtration Apparatus, and Pumping Parameters

Principal component analysis revealed two significant components (eigenvalue < 1) explaining 76.1% of the total variation (**Figure 2**). The first principal component showed strong associations with the number of choanocytes per chamber (*nc* CC^{-1}), choanocyte chamber size (CC diameter), AFDW, and porosity. The vectors representing these variables were close to each other indicating a positive relationship with each other. Additionally, the vectors were oriented toward sponge species with high scores on these variables (example–*Callyspongia* sp. and *I. fusca*). Variables related to the structural components such as tissue density, spicule volume, and inorganic contents (ash%) were positioned along with the second component and their vectors were oriented toward species scoring high on these variables (*C.* cf. *cavernosa* and *B. fortis*).

The angles between the vectors on the PCA loading plot indicated a potential relationship between the variables and were further examined on Pearson's correlation matrix (**Figure 3A**). In general, the variables related to the filtration apparatus (CC mm^3, CC diameter, and the number of choanocytes per chamber (*ncc*) CC^{-1}, and porosity%) showed a positive correlation with the pumping parameters (excurrent velocity mm s^{-1} and pumping rate ml s^{-1} ml^{-1}) and a negative correlation with structural components (density, ash mass%, and spicule volume proportion%). Particularly, the number of choanocytes per chamber (*ncc* CC^{-1}) showed a significant positive correlation with the pumping rate ($r = 0.77$, $n = 7$, $p < 0.05$). Note that within the structural components, the density–porosity, the ash mass%, AFDW% have a naturally inverse association. Interestingly, this was reflected in their relationship with the variables related to the pumping parameters and the filtration apparatus. For instance, *ncc* CC^{-1} had a significant positive correlation with AFDW%, but a significant negative correlation with Ash%. Similarly, spicule volume which had a significant positive correlation with tissue density had a significant negative correlation with porosity ($r = -0.93$, $n = 7$, $p < 0.001$). This indicated that spicules can form notable intrusions in the water passages and pores of the sponge aquiferous system (**Figure 3B**). For example, *Calyspongia* sp. showed distinctive lacunar spaces around CC, and *I. fusca* had the largest CC and both the sponges had high porosity and low spicule contents (**Figures 3C,D**).

Sponge Pumping Parameters

Mean excurrent velocity and pumping rate with respect to the sponge biovolume and dry mass of the studied species is given in **Table 1**. Both excurrent velocity and the oscular flow rates showed a positive relationship with the OSA

TABLE 1 | Mean excurrent velocity and pumping parameters of the studied species.

Species	Number of specimens (n)	Excurrent velocity (mm s^{-1})	Pumping rate (ml s^{-1} ml^{-1} sponge)	Pumping rate (ml s^{-1} g^{-1} DWsponge)
Amorphinopsis foetida	3	13.44± 0.83	0.04 ± 0.01	0.54 ± 0.09
Beimna fortis	5	–	–	–
Calyspongia sp.	5	28.83± 1.38	0.33 ± 0.05	1.85 ± 0.43
Cinachyrella cf. *cavernosa*	9	27.59 ± 1.46	0.05 ± 0.005	0.07 ± 0.01
Haliclona sp.	5	11.03 ± 0.34	0.11 ± 0.01	0.65 ± 0.09
Ircinia fusca	7	33.46 ± 1.06	0.12 ± 0.02	0.41 ± 0.06
Suberites carnosus	5	35.54 ± 0.75	0.23 ± 0.01	1.68 ± 0.03

Data are means ± SE pumping rate is standardized by sponge volume (per ml sponge) and sponge weight [per gram dry weight (DW)].

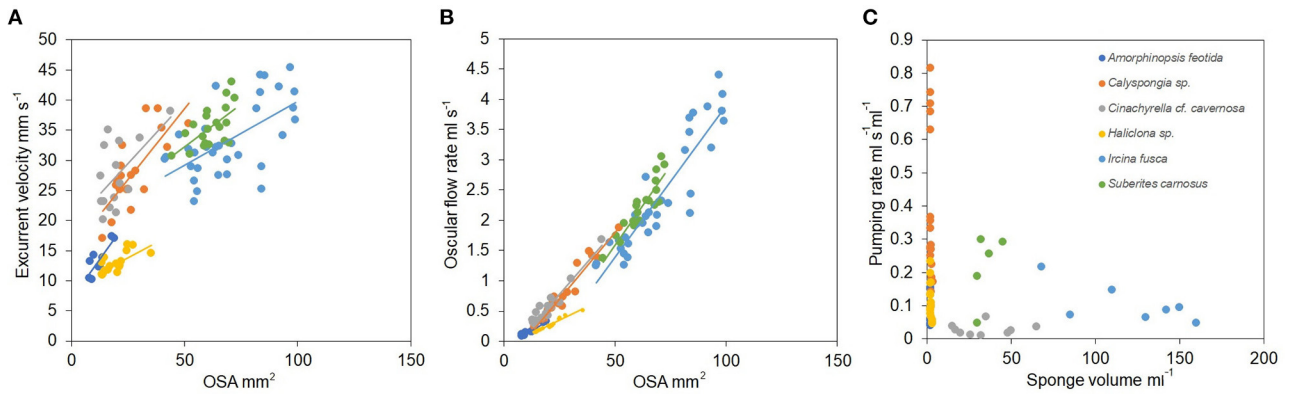

FIGURE 4 | (A) Relationship between the excurrent velocity (mm s^{-1}) and the osculum cross sectional area (mm^2). **(B)** Relationship between the oscular flow rate (ml s^{-1}) and the oscular cross sectional area (mm^2). **(C)** Pumping rate (ml s^{-1} ml^{-1}) vs. sponge volume (ml).

TABLE 2 | The relationship of excurrent velocity and oscular flow rate with the oscular cross sectional area of the studied sponges assessed with linear regression.

Species	Excurrent velocity						Oscular flow rate					
	n	*F*	Constant	*B*	R^2	*p*	*N*	*F*	Constant	*B*	R^2	*p*
Amorphinopsis feotida	9	17.25	6.97	0.52	0.71	0.004	9	163.50	−0.092	0.02	0.95	<0.001
Calyspongia sp.	19	22.10	15.03	0.47	0.56	<0.001	19	242.83	−0.40	0.04	0.93	<0.001
Cinachyrella cf. cavernosa	15	6.61	19.37	0.40	0.33	0.023	15	166.60	−0.27	0.04	0.92	<0.001
Haliclona sp.	20	19.75	8.92	0.19	0.52	<0.001	20	349.45	−0.08	0.01	0.95	<0.001
Ircinia fusca	33	17.82	18.47	0.21	0.36	<0.001	33	160.52	−1.10	0.05	0.83	<0.001
Suberites carnosus	20	11.62	17.95	0.28	0.39	0.003	20	87.84	−1.03	0.05	0.83	<0.001

n is the number of oscula.

(**Figures 4A,B** and **Table 2**). Note that species that clustered tightly around the regression line, such as *Haliclona* sp. had small, non-contractile, and consistent oscular size within and between different individuals of different sizes, whereas species with high deviations from the regression line such as *I. fusca*, *C.* cf. *cavernosa* had contractile oscula with variable size within and between individuals. The volume of water processed per ml of sponge, i.e., the size-specific pumping rate, decreased with sponge volume for all the studied species (**Figure 4C**).

Sponge Body Composition

Mean values for the filtration apparatus [CC mm^3, CC diameter, and the number of choanocytes per chamber (*ncc*) CC^{-1}, and porosity %] and the structural components (density, ash mass%, AFDW%, and spicule volume proportion%) of the studied species is given in **Table 3**. For most of the species, the ash% was more than 50% of the dry weight. The proportion of the total volume occupied by spicules/inorganic material ranged from 3 to 9% (**Figure 5A**) and also showed a significant positive relationship with the tissue density (DW/volume) (*r*

TABLE 3 | Mean values of the structural components and the filtration apparatus of the studied species.

Species	Density (Dry W/vol)	Ash% dry weight	Porosity %	Spicules% (Volume proportion)	AFDW %	CC diameter (um)	CC mm^3	*ncc* CC^{-1}
Amorphinopsis foetida	0.16 ± 0.01	53.14 ± 7.07	52 ± 2.83	4.23 ± 0.45	46.85 ± 7.69	17.46± 0.13	3690.67± 87.49	84.11 ± 3.02
Biemna fortis	0.26 ± 0.01	52.41 ± 6.22	38.5 ± 2.75	6.73± 1.04	47.58± 6.22	17.18±0.42	2781.85± 242.20	35.02 ± 2.44
Calyspongia sp.	0.13 ± 0.01	42.20 ± 4.38	56 ± 2.39	2.80 ± 0.19	57.79 ± 2.74	19.35±0.2	3452.09±113.17	121.11 ± 4.33
Cinachyrella cf. *cavernosa*	0.28. ± 0.01	65.71 ± 1.27	30 ± 2.09	8.73 ± 0.67	34.28 ± 4.82	18.62±0.21	4482.82 ±81.48	51.87 ± 3.77
Haliclona sp.	0.11 ± 0.008	50.00 ± 1.56	54.51 ± 2.08	2.80 ± 0.18	49.99 ± 1.56	19.69±0.23	3301.86 ±118.31	68.83 ± 2.82
Ircinia fusca	0.25 ± 0.01	36.97 ± 2.93	52.45 ± 0.96	4.32 ± 0.39	63.02± 2.93	30.68±0.29	3052.59 ±92.39	120.35± 8.98
Suberites carnosus	0.23 ± 0.01	47.96 ± 7.61	35 ± 2.02	5.60 ± 1.27	52.03 ± 7.61	16.21±0.23	5736.16 ±51.82	84.21 ± 3.82

Data are means ± SE.

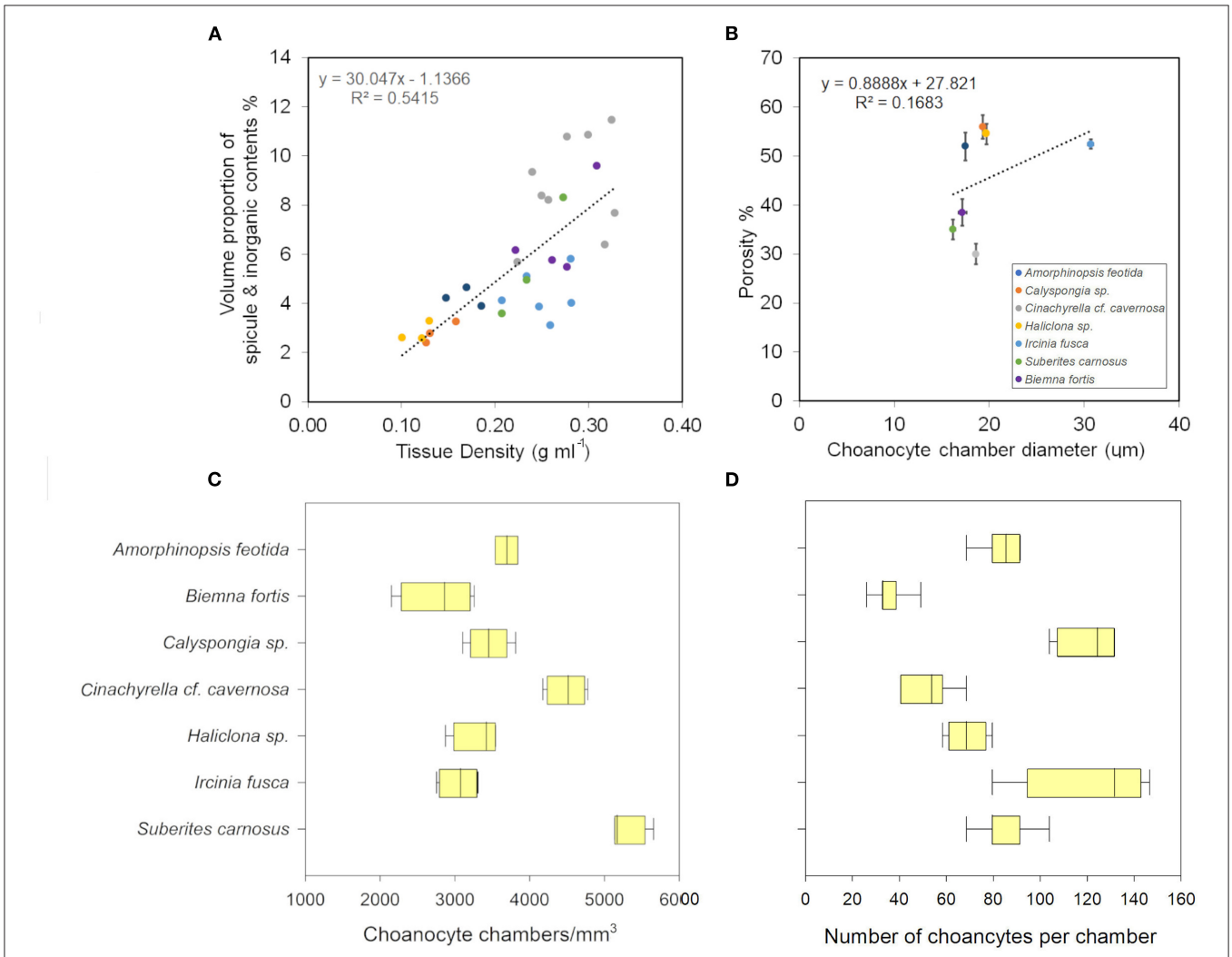

FIGURE 5 | (A) Volume of sponge tissue occupied by spicules (%) increases as the tissue density increases. **(B)** Porosity and the choanocyte chamber diameter show a positive relationship. **(C)** The choanocyte chamber abundance in different sponges. **(D)** The number of choanocytes per chamber in different sponges.

= 0.73, n = 31, p < 0.001). This suggests that the spicules constitute a major portion of sponge dry weight and also sponge volume. Porosity in the form of canals and pores between the collagen fibers, cells, and mesohyl matrix ranged from 30 to 55 % for the studied sponges and showed a positive relationship with the choanocyte diameter (**Figure 5B**), although

TABLE 4 | A pairwise comparison (Tukey test) of the mean differences between the sponge species with respect to the dependent variables: filtration apparatus (CC mm^3, *ncc* CC^{-1}, CC diameter) and structural components (ash%, AFDW%, porosity%, density, and spicule volume%).

	Amorphinopsis feotida	***Biemna fortis***	***Calyspongia* sp.**	***Cinachyrella* cf. *cavernosa***	***Haliclona* sp.**	***Ircinia fusca***	***Suberites carnosus***
CC mm^3							
Amorphinopsisfeotida	–	**908.82**	238.57	**758.95**	388.80	**638.08**	**1590.98**
Biemna fortis		–	**670.24**	**1667.77**	520.01	270.73	**2499.80**
Calyspongia sp.			–	**997.53**	150.22	399.50	**1829.56**
Cinachyrella cf. *cavernosa*				–	**1147.75**	**1397.03**	**832.03**
Haliclona sp.					–	249.27	**1979.79**
Irciniafusca						–	**2229.06**
Suberites carnosus							–
nccCC^{-1}							
Amorphinopsisfeotida	–	**42.70**	**42.36**	27.98	10.96	**36.74**	6.02
Biemna fortis		–	**85.07**	14.72	**31.74**	**79.44**	**48.73**
Calyspongia sp.			–	**70.35**	**53.33**	5.62	**36.34**
Cinachyrellacf. cavernosa				–	17.02	**64.72**	**34.01**
Haliclona sp.					–	**47.70**	16.98
Irciniafusca						–	**30.71**
Suberites carnosus							–
CC diameter							
Amorphinopsisfeotida	–	2.26	2.56	2.30	3.43	**12.50**	0.69
Biemna fortis		–	0.29	0.04	1.17	**10.24**	1.56
Calyspongia sp.			–	0.25	0.87	**9.94**	1.86
Cinachyrellacf. cavernosa				–	1.12	**10.19**	1.61
Haliclona sp.					–	**9.07**	2.73
Irciniafusca						–	**11.81**
Suberites carnosus							–
Ash							
Amorphinopsisfeotida	–	0.86	11.11	**20.93**	3.22	16.35	5.40
Biemna fortis		–	**10.25**	**21.79**	2.36	15.48	4.45
Calyspongia sp.			–	**32.04**	7.88	5.23	5.70
Cinachyrellacf. cavernosa				–	**24.1**	**37.28**	**26.33**
Haliclona sp.					–	13.12	2.17
Irciniafusca						–	10.94
Suberites carnosus							–
AFDW							
Amorphinopsisfeotida	–	5.6	15.87	16.17	7.98	**21.10**	10.16
Biemna fortis		–	10.25	**21.79**	2.36	15.48	4.54
Calyspongia sp.			–	**32.04**	7.88	5.23	5.70
Cinachyrella cf. *cavernosa*				–	**24.15**	**37.28**	**26.33**
Haliclona sp.					–	13.12	2.17
Irciniafusca						–	10.94
Suberites carnosus							–
Porosity							
Amorphinopsisfeotida	–	**13.50**	3.33	**21.25**	**2**	0.33	**17**
Biemna fortis		–	**16.83**	7.75	**15.50**	**13.83**	3.50
Calyspongia sp.			–	**24.58**	1.33	3	**20.33**
Cinachyrella cf. *cavernosa*				–	**23.35**	**21.58**	4.28
Haliclona sp.					–	1.66	**19**
Irciniafusca						–	**17.33**
Suberites carnosus							–

(Continued)

TABLE 4 | Continued

	Amorphinopsis feotida	*Biemna fortis*	*Calyspongia* sp.	*Cinachyrella*cf. *cavernosa*	*Haliclona* sp.	*Ircinia fusca*	*Suberites carnosus*
Density							
Amorphinopsisfeotida	–	**0.09**	0.02	**0.12**	0.05	**0.08**	0.07
Biemna fortis		–	**0.12**	0.02	**0.14**	**0.01**	0.02
Calyspongia sp.			–	**0.15**	**0.02**	**0.11**	**0.09**
Cinachyrella cf. *cavernosa*				–	**0.17**	0.03	0.05
Haliclona sp.					–	**0.13**	**0.12**
Irciniafusca						–	0.01
Suberites carnosus							–
Spicule volume							
Amorphinopsisfeotida	–	2.49	1.43	6.07	1.42	0.08	1.36
Biemna fortis		–	**3.92**	**3.57**	**3.92**	**2.41**	1.13
Calyspongia sp.			–	**7.50**	0.00	1.51	2.79
*Cinachyrella*cf. *cavernosa*				–	**7.50**	**5.98**	**4.70**
Haliclona sp.					–	1.51	2.79
Irciniafusca						–	1.27
Suberites carnosus							–

Significant differences ($p < 0.05$) are in bold.

the relationship was not significant. The abundance of the CC and the number of the choanocytes per chamber showed high variation between the studied species (**Figures 5C,D**). The multivariate analysis indicated a significant difference between examined species with respect to the variables related to filtration apparatus (CC mm^3, *ncc* CC^{-1}, CC diameter) and structural components (ash%, AFDW%, porosity%, density, and spicule volume%) (MANOVA, Wilks test 0.00, $F = 9.08$, $p < 0.001$). *Post-hoc* Tukeys HSD test was performed to examine individual mean difference comparisons across all studied sponge species. Statistically significant ($p < 0.05$) mean differences between the species are presented in **Table 4**. Several factors influenced the abundance of choanocyte chambers. The least number of CC were found in *B. fortis*. The buried growth form of the sponge showed very sparse cellular tissue after the dissolution of the spicules and sand grain inclusions (**Figure 6**). *I. fusca* and *A. foetida* showed several spermatic cysts in different stages of development, which may have affected the abundance of CC (**Figure 6**). The histological sections of *Calyspongia* sp. showed a loose organization of cells and CC along with the elements of the collagen skeletal framework (**Figure 6**).

Morphometric Analysis

Dimensions of the aquiferous structures for the sponges included in the present investigation are given in **Table 5**. Sponge morphology and growth form affected the distribution and abundance of the components of the aquiferous system. For example, for the buried growth form of *B. fortis*, the surface in current pores, ostia, were observed on the fistules growing above the ground, and for *C.* cf. *cavernosa* the ostia were restricted to the rounded depression/pits called porocalices present on the lateral surfaces around the base of the sponge (**Figures 7A,B**). Ostia was observed to be in varying states of contraction (**Figures 7C,D**). The CC in *C.* cf. cavernosa was set in densely packed mesohyl, which was interspersed with several large spherulous cells (**Figure 8A**). The CC opened into the excurrent canals *via* the apopyle (**Figures 8B–D**). A glycocalyx mesh and flat gasket like structure around the choanocyte microvilli are likely to be a common occurrence in the demosponges; however, these structures are usually very difficult to preserve (Ludeman et al., 2016) and could not be observed clearly due to poor preservation. The largest CC was observed in *I. fusca* (**Figure 8E**).

Transmission Electron Microscopy

No microbial cells were detected in the TEM micrographs of *Halicona* sp., *Calyspongia* sp., *A. foetida,* and *S. carnosus* (**Figures 9A–D**). In contrast, a high number of bacterial cells was detected in TEM micrographs of *I. fusca* (**Figure 9E**). The bacterial cells had diverse morphotypes and were located extracellularly in the sponge mesohyl. *B. fortis* and *C.* cf. *cavernosa* showed moderate to few bacterial cells in the mesohyl, respectively (**Figures 9F,G**). Additionally, various cell types were observed in the TEM micrographs. Choanocytes in the *Halicona* sp. were spherical or oval in shape and measured 3.2–4 μm in size. Several larger cells with a nucleolated nucleus, almost double the size of the choanocytes, were also detected. *Calyspongia* sp. showed large cells 10–11 μm in size and with a high number of oval-shaped inclusions (**Figure 9B**), suggesting the possibility of mucus-secreting cells. Oval-shaped archeocytes having a nucleus with the distinct nucleolus and a well-developed endoplasmic reticulum could be seen in the *A. foetida* (**Figure 9C**). Large irregularly shaped cells with several spherical

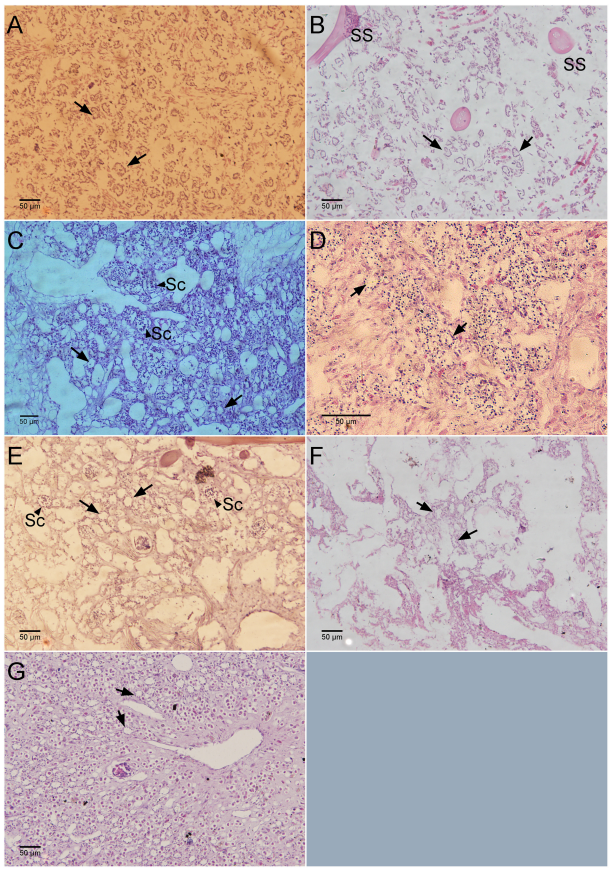

FIGURE 6 | Histological sections showing the number of chaonocyte chambers per view field. **(A)** *Haliclona* sp., **(B)** *Calyspongia* sp., **(C)** *Amorphinopsis foetida,* **(D)** *Suberites carnosus,* **(E)** *Ircinia fusca,* **(F)** *Biemna fortis,* **(G)** *Cinachyrella* cf. *cavernosa.* Black arrows point toward the choanocyte chambers. The black arrow head indicates the sperm cysts (Sc). SS, Spongin skeleton.

shaped and electron-dense inclusions were seen in *S. carnosus* (**Figure 9D**).

DISCUSSION

Sponge Species and the Variations in the Proportions of the Structural Components

Several intrinsic factors such as microbial abundance (Weisz et al., 2008), sponge shape (McMurray et al., 2014), osculum contraction (Hadas et al., 2008; Strehlow et al., 2016; Kumala et al., 2017; Goldstein et al., 2019), canal system (Reiswig, 1975), and the number of CC (Massaro et al., 2012) are known to influence sponge pumping rate. However, recent studies show sponge volume as the major factor to influence the size-specific pumping rate, i.e., the pumping rate normalized to the sponge volume (Morganti et al., 2019, 2021). The differences in the size-specific pumping rates of different sized individuals within and between species can transcend the effects of some of the distinctions such as HMA–LMA dichotomy on sponge pumping. Although HMA sponges are generally large and fleshy (Gloeckner et al., 2014) and have higher volume compared with LMA sponges (Morganti et al., 2019, 2021), the increase in the structural component of the mesohyl and tissue density results in the reduction of the hollow structures of the aquiferous system. In the present study, we examined the structural and functional variation in the anatomical and morphological characteristics of seven sponge species. PCA analysis of the variables related to the structural components, filtration apparatus, and pumping parameters revealed a scatter plot of the sponge species driven by the relationships between these variables (**Figure 2**). The structure and the efficiency of the filtration system show huge interspecific variation in sponges and are related to biological strategies in response to environmental conditions (Turon et al., 1997). The sponge species selected in the present study involve diverse modifications in terms of morphological growth forms (buried, globular, massive) and anatomical variations in terms of quantity of spicule skeleton, mesohyl proportion, and dimensions of the aquiferous structures.

Dimensions of the Aquiferous Structures in the HMA and LMA Sponges Vary With Respect to the Proportion of Spicules

In the present study, TEM images of *I. fusca*, *B. fortis,* and *C.* cf. *cavernosa* showed a high to a moderate abundance of microbes in the mesohyl, respectively. Although the high abundance of microbes in the *I. fusca* indicates a higher proportion of mesohyl and cellular mass, as represented by the high AFDW%, the tissue density remained moderate (**Table 3**). Histological sections and SEM images showed that *I. fusca* had the largest CC compared with other species studied in the present investigation. In demosponges, the size and volume of the choanocyte chamber vary between species, and keratose sponges are known to have large choanocyte chamber volumes (Vacelet et al., 1989). These sponges also lack mineral spicule skeletons (Bergquist, 1978; Maldonado, 2009; Erpenbeck et al., 2012). The absence of spicules along with large CC counterbalance the higher proportion of mesohyl and maintain a high pumping rate of *I. fusca* compared with other sponges, which were mainly LMA (**Figure 4**).

Sponges acquire the mesohyl microsymbionts *via* vertical transmission as well as horizontal/environmental transmission (Schmitt et al., 2007; Webster et al., 2010; Turon et al., 2018). Vertical transmission of microbes indicates that the mesohyl densely packed with microbes, characteristic of HMA sponges, is present from larval stages. The microbial communities are temporally stable in both HMA/LMA sponges (Taylor et al., 2007; Gloeckner et al., 2014; Erwin et al., 2015), suggesting that the mesohyl characteristics are preserved. Additionally, studies show that HMA sponge *Geodia barreti* phagocytose symbiont microbes in a controlled manner (Leys et al., 2018), indicating the microbial abundance in the mesohyl is maintained. However, the proportion of spicules and the filtration components vary with the sponge growth and reproductive seasons. For instance, the

TABLE 5 | Dimensions of the components of the aquiferous system calculated from the SEM and histological images of the study species.

Aquiferous structures	*Amorphinopsis foetida*	*Biemna fortis*	*Calyspongia* sp.	*Cinachyrella* cf. *cavernosa*	*Haliclona* sp.	*Ircinia fusca*	*Suberites carnosus*
Ostia (area μm^2)	138.99	707.7508	730.38	647.45	430.67	239.56	38.05
Subdermal spaces (diameter μm^2)	25084.58	15689.93	13891.48	65354.63	4908.92	78282.41	45791.22
Large incurrent canals (diameter μm)	10688.02	22338.30	2840.24	1800.18	3685.68	39268.21	1257.98
Medium incurrent canals (diameter μm)	2849.97	5291.09	7304.40	985.09	1407.26	6856.69	892.56
Small incurrent canals (diameter μm)	1863.25	176.74	1708.22	293.25	758.35	820.94	741.22
Choanocyte chambers (area μm^2)	245.86	232.19	301.23	272.97	303.28	665.28	220.93
Apopyle (area μm^2)	124.11	–	168.54	–	113.21	211.25	–
Small excurrent canals (diameter μm)	2174.32	454.89	1355.85	371.38	879.42	783.41	691.75
Medium excurrent canals (diameter μm)	3485.21	1207.65	5864.75	1571.24	1562.34	7644.56	834.15
Large excurrent canals (diameter μm)	8662.71	11968.58	6142.35	20781.25	4235.71	26218.21	2784.68
Osculum (area mm^2)	21.24	56.34	18.01	31.59	7.32	73.31	19.65

distribution and the proportions of tissue (mesohyl), spicules, and the aquiferous system vary between different stages of development, as observed in the developing buds of sponge *Tehya wilhelma* (Hammel et al., 2009). Thus, the proportion of spicule content and the aquiferous system is more likely to vary in different sized individuals within the species than the microbial abundance in the mesohyl. These considerations seem compatible with the wide range of size-specific pumping rates observed in the different sized individuals of HMA and LMA sponges (Morganti et al., 2019, 2021).

Recent studies evaluated a large number of sponge species for their HMA/LMA status (Gloeckner et al., 2014; Moitinho-Silva et al., 2017). Moreover, new methods and techniques like machine learning algorithms are being developed and employed to cover a large number of sponge species to predict their HMA-LMA status (Moitinho-Silva et al., 2017). Sponge species along the Indian coast have not been evaluated for their HMA-LMA status. TEM analysis showed low microbial abundance for the sponges *Haliclona* sp., *Calyspongia* sp., *A. foetida*, and *S. carnosus*. Bacterial cells were found to have moderate to high abundance in sponges *Cinachyrella* cf. *cavernosa*, *B. fortis,* and *I. fusca*. The microbial abundance in sponge mesohyl represented by the HMA–LMA dichotomy is best described as a continuum with a highly bimodal distribution, where most species are found at the extreme ends, and few species show an intermediate microbial load (Gloeckner et al., 2014). However, for sponges with intermediate bacterial abundance, TEM analysis alone is not sufficient to determine if the species is HMA or LMA (Gloeckner et al., 2014). Therefore, the HMA and LMA status of the sponge species in the present investigation need to be further determined by additional techniques such as 16 s rRNA gene sequence data.

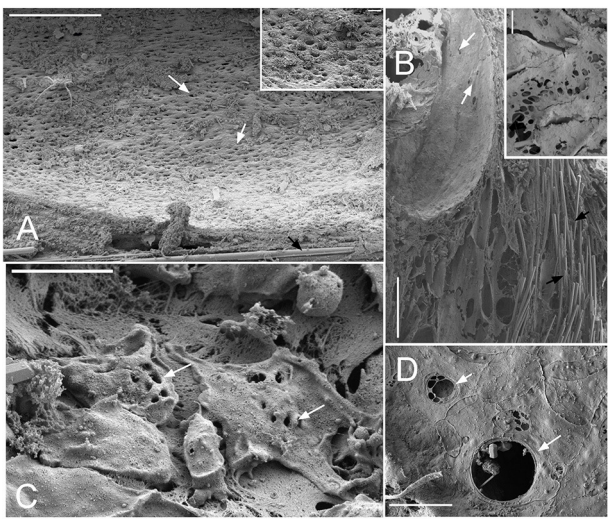

FIGURE 7 | SEM images showing the ostia **(A)** *Cinachyrella* cf. *cavernosa* the incurrent pores, ostia, are present in rounded depression/pits of the porocalices on the lateral surfaces along the base of the sponge. Inset magnified view of the ostia. **(B)** For the buried growth form of *Biemna fortis,* the ostia present on the fistules/finger-like projection growing above the ground. Inset magnified view of ostia **(C)** *Suberites carnosus* porocytes with ostia **(D)** *Amorphinopsis foetida* ostia. The white arrows point to the ostia. Scale bars: **(A)** 500 μm, inset = 50 μm; **(B)** 500 μm, inset 50 μm; **(C)** 20 μm; **(D)** 5 μm.

Spicule (Weight and Volume) Form a Major Component of Tissue Density and Have an Inverse Relationship With Porosity

Spicules form important support structures assembled into large pole-and-beam formations with a variety of morphologies (Uriz, 2006). In the sponge *Ephydatia muelleri* the spicules are secreted and carried by specialized cells to the distant assembly locations and held up along their long axis (Nakayama et al., 2015). Such spicule tracts support the apical pinacoderm, which is raised and lowered during the contraction events, like a diaphragm, reducing the volume of the subdermal space (Elliott and Leys, 2007). Such mechanisms indicate that spicules have an important role in sponge body contractions. Although spicules themselves form a non-contractile component of the sponge

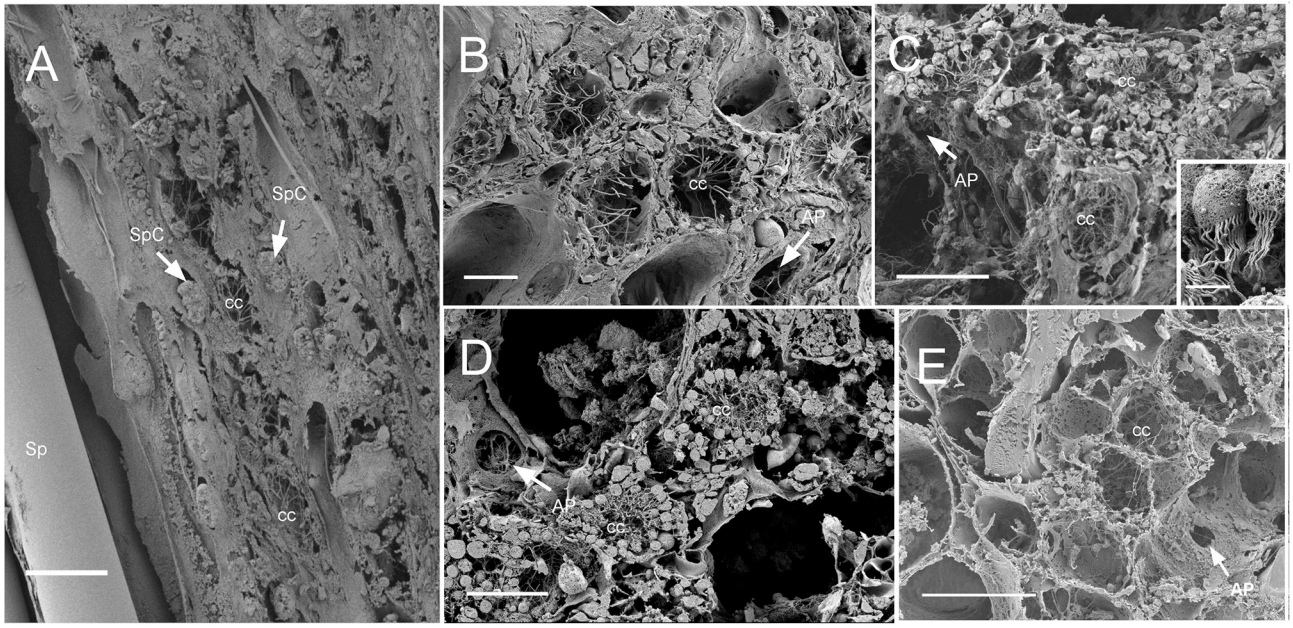

FIGURE 8 | SEM of chaonocyte chambers. **(A)** The choanocyte chambers (CC) and the spherulous cells (SpC) are present in the sponge *Cinachyrella* cf. *cavernosa*, spicules are indicated with sp. **(B)** The CC in *Amorphinopsis foetida*. The apopyle (AP) is indicated with a white arrow. **(C)** *Calyspongia* sp. with the choanocyte chamber (cc) and the apopyle (AP) indicated with a white arrow. The inset shows a closeup of the choanocytes with the flagella and microvillar collar, individual microvilli can be seen connected with glycocalyx mesh. **(D)** *Haliclona* sp. CC and the flagella of another choanocyte chamber seen through Apopyle (AP) indicated with white arrow. **(E)** *Ircinia fusca* CC and the apopyle (AP). Scale bar: **(A)** 20 μm; **(B)** 10 μm; **(C)** 20 μm, inset 2 μm; **(D)** 20 μm; **(E)** 50 μm.

body, their weight and position likely help to collapse the hollow spaces within the sponge during contraction. In fluid transport systems, architectural characteristics like porosity, pore size, and permeability of the biological scaffold, play a significant role in flow transport (Hollister, 2005). The increase in the spicule skeleton weight was a major contributor to the tissue density (and decrease porosity) as represented by the ash mass% (**Table 3** and **Figure 5**). Also, the volume proportion of the spicules within the tissue showed a significant positive correlation with the density (**Figure 5**) and a significant negative correlation with porosity%. The high porosity observed in *Haliclona* sp. and *Calyspongia* sp. could be attributed to the combination of low spicule contents and the presence of several lacunar spaces, which contained the choanocyte chambers, canals, and the loose organization of the cells. Porosity is a measure of the void fraction in material, and these voids can either be "closed" or "open" and connected to other voids and thence to the exterior of the material (Lawrence and Jiang, 2017). The internal and external surfaces of sponges are covered by pinacoderm which is made of flat cells called pinacocytes. Sponges are known to actively close and open the oscula and ostia present on the pinacoderm, thus effectively regulating the water flow (Nickel, 2004, 2010; Ellwanger and Nickel, 2006; Elliott and Leys, 2007; Ludeman et al., 2014; Goldstein et al., 2020). Some species show a flow-regulating cell type "reticuloapopylocyte" at the apopylar opening of the CC, suggesting a possibility of flow control mechanism at the level of individual CC and their connecting canals (Hammel and Nickel, 2014; Ludeman et al., 2016). Several sponge species are capable of coordinated contractions (Nickel, 2010), and pinacoderm acts as a major conductive pathway during contraction processes which lead to the collapse of the internal void spaces in the form of in and excurrent canals and the subdermal cavities (Hammel et al., 2012; Goldstein et al., 2020). Thus, sponges control the surface pores, as well as the internal porosity, and effectively manage the volume of water pumped and filtered.

Actively pumping sponges generate a water current by the beating action of the choanocyte flagella in the choanocyte chambers. It has been suggested that the pumping rate could be correlated to the abundance of CC (Riisgård et al., 1993). However, CC is a dynamic structure with a high proliferation activity and cell shedding of choanocytes (De Goeij et al., 2009; Luter et al., 2012; Alexander et al., 2014). Additionally, gametogenesis in some sponges involves the conversion of choanocytes into reproductive cells (Shore, 1971; Simpson, 1984; Tanaka-Ichihara and Watanabe, 1990; Tsurumi and Reiswig, 1997; Ereskovsky and Gonobobleva, 2000). Several sperm cysts were observed in the histological sections of *A. foetida* and *I. fusca* (**Figure 6**), and such mechanisms are likely to affect the abundance of chaonocyte chambers within the tissue and also the number of choanocytes within the chambers. In the present investigation, the formula used for calculating the number of choanocytes within the chamber (*ncc* CC^{-1}) does not consider the apopyle and the porospyle. Therefore, the formula

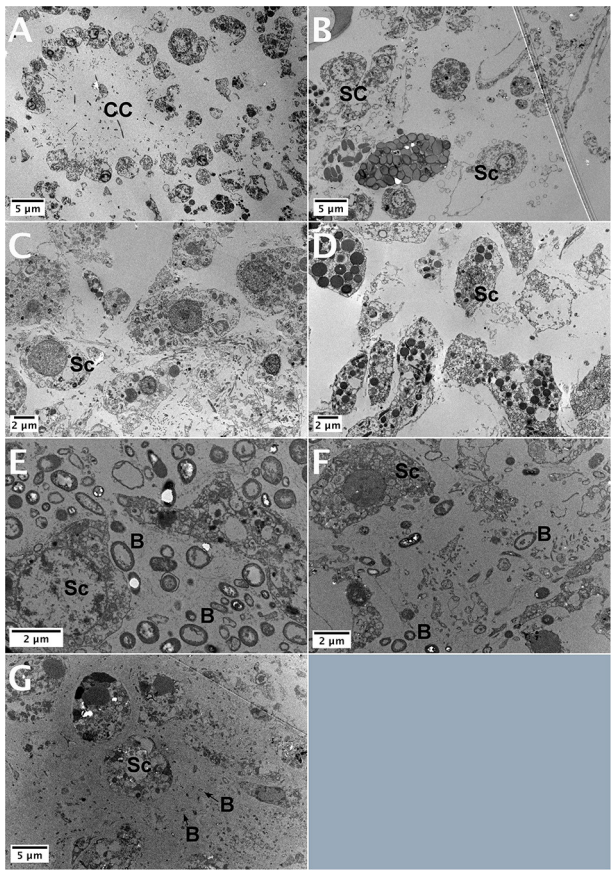

FIGURE 9 | TEM images of the study sponges **(A)** *Haliclona* sp., **(B)** *Calyspongia* sp., **(C)** *Amorphinopsis foetida,* **(D)** *Suberites carnosus,* **(E)** High abundance of bacterial cells present in the *Ircinia fusca* mesohyl, **(F)** *Biemna fortis,* and **(G)** *Cinachyrella* cf. *cavernosa* showing a moderate abundance of bacterial cells in the mesohyl. CC, choanocyte chamber; Sc, sponge cell; B, bacterial cell.

estimates the maximum number of choanocytes present within the chamber and showed large differences between the species ranging from 35.02 ± 2.44 (*C.* cf. *cavernosa*) to 121.11 ± 4.33 (*Calyspongia* sp.), majorly due to the different sized chambers between the species (**Table 3** and **Figure 3**). Interestingly, the *ncc* CC^{-1} showed a significant positive correlation with the AFDW%, indicating that the number of choanocytes within the chamber increased with the percentage of the organic/cellular material in the dry weight of the sponge sample (AFDW). Choanocytes are one of the most common and prominent cell types in sponges (Funayama et al., 2005; Riisgård et al., 2016) and most of the species in the present study showed a low or total absence of microbes in the mesohyl (except *I. fusca*) (**Figure 9**), implying that the AFDW% in the dry sponge samples represented the sponge cellular material. Theoretical estimates and experimental studies on small sponge explants suggest that the CC has a uniform distribution within the sponge tissue and has similar individual pumping rates (Reiswig, 1975; Riisgård et al., 2016; Goldstein et al., 2019). The distribution of the CC within the sponge and abundance of the chambers in different-sized individuals is likely to depend on the proportion of the structural and aquiferous components. The modularity of sponges is defined by the aquiferous modules which are described as a system of CC and aquiferous canals associated with a single osculum (Fry, 1970, 1979; Ereskovskii, 2003) (**Figure 10A**). However, the aquiferous structures and the proportion of the structural components (mesohyl and spicule skeleton) between different aquiferous modules may differ between different parts of the sponge and between different-sized individuals.

The Distribution of the Aquiferous Structures Is Influenced by the Sponge Morphology

The distribution of the aquiferous structures was governed by the morphological characteristics of the sponge (**Figures 10A,B**). For instance, the ostia restricted to the porefields porocalices situated laterally along the base of the spherical shaped sponge *C.* cf. *cavernosa* indicates the components of the aquiferous system do not have a homogenous distribution pattern (**Figure 10C**). Similarly, *B. fortis* had a buried growth form and high proportions of inclusions of inorganic debris in the buried portion with elongated, finger-like apical extensions or fistules visible above ground, which did not show any pumping activity. Sediment dwelling sponge species often show physiological and morphological adaptations to their environment (Ilan and Abelson, 1995; Schönberg, 2016). A previous study on sponge *Biemna ehrenbergi* reported the presence of ostia mostly on the buried surface of sponge, and it was also observed that the dye injected into the sediment was pumped and expelled through the oscula present on the chimney like siphons that protrude from the sediment surface (Ilan and Abelson, 1995). However, it is also suggested that sponges that inhabit soft sediments may have a reverse mechanism in which water flow is directed from the fistules into the sediments (Schönberg, 2016). Studies on sediment dwelling in *Oceanap iaoleracea* and *Oceanap iapeltata* report that both these species possess inhalant siphons, which draw water from above the sediment surface and conduct it to the central body, buried in the sediments (Werding and Sanchez, 1991). In the present study, for *B. fortis*, the ostiawere observed on the surface of the siphons exposed above the sediments, which suggests that the water enters the sponge *via* the fistules and siphons exposed above the ground and is pumped into the sediments by the buried portion of the sponge body.

CONCLUSION

In sponges, the proportion between the weight of tissues and the distribution and arrangement of the components of the aquiferous system leads to the optimization of some physiological factors (Ereskovskii, 2003). The sponge body has a characteristic of a composite material with a flexible matrix

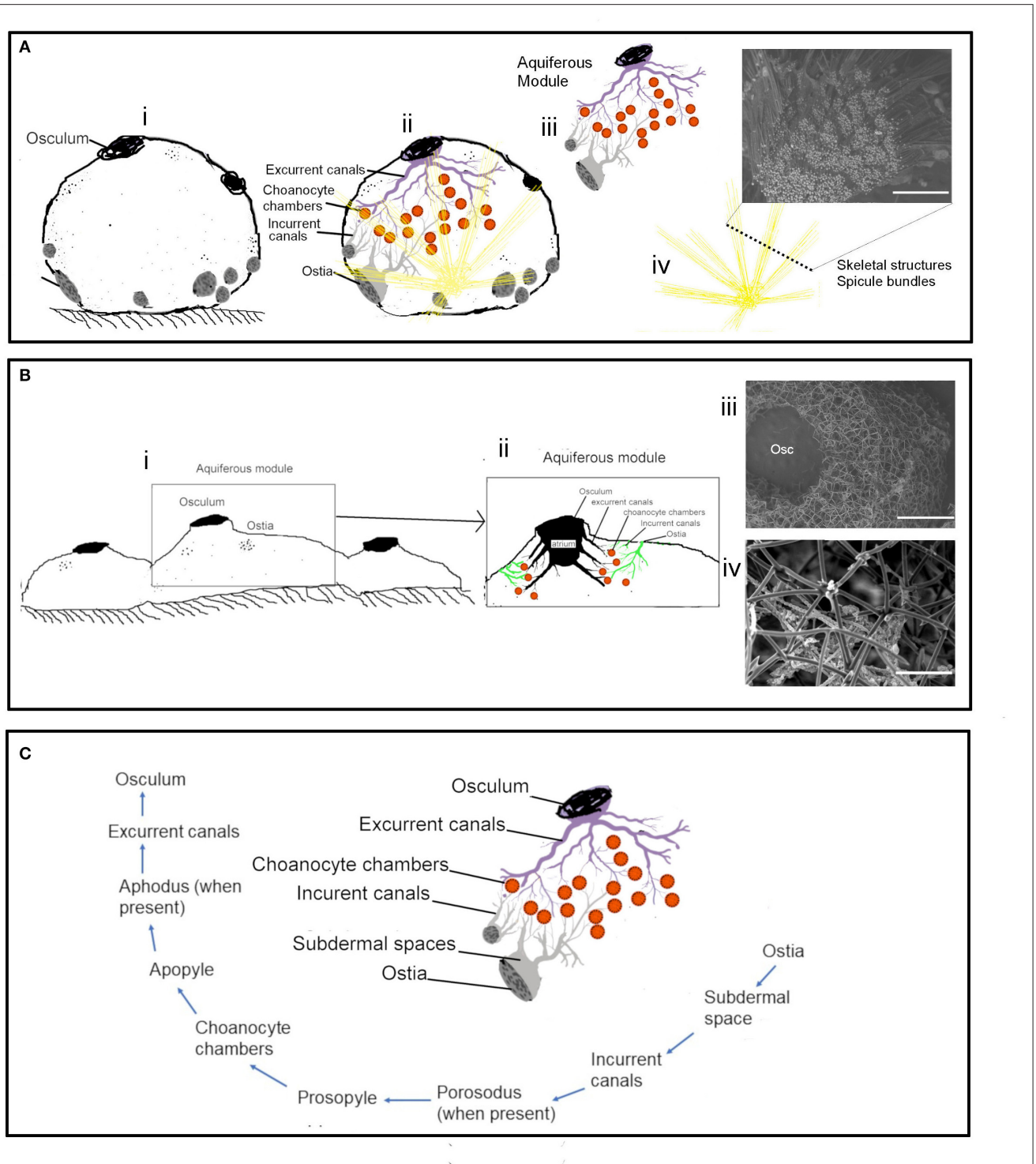

FIGURE 10 | The aquiferous system and the skeletal system in different morphologies: **(A)** Schematic representation of the spherical-shaped sponge *Cinachyrella* cf. *cavernosa* (i) the aquiferous system associated with a single osculum and the skeletal structures with the radiating spicule bundles (ii). the functional unit of the aquifeorus system-aquiferous module (iii). The skeleton of radiating spicule bundles, the dotted line represents a transverse section of the spicule bundles as seen in an SEM (iv). **(B)** Encrusting morphology of sponge (i). Aquiferous module (ii) with the SEM of the skeleton structure of *Calyspongia* sp. (iii) and *Haliclona* sp. **(C)** The components of an aquiferous module and the path of the water through the aquiferous system of sponge.

of tissue, organic (spongin) with inclusions of an inorganic skeleton (spicules or incorporated foreign material) (Palumbi, 1986). Shifting proportions of these materials change the properties of a sponge body to being more elastic with an increase in spongin, whereas an increase of inorganic skeleton makes the sponge harder and more resistant to physical forces (Palumbi, 1984, 1986; Sim and Lee, 2002; Uriz et al., 2003). Sponges with higher tissue density are known to have a reduced aquiferous system in form of narrower canals, fewer chaonaocyte chambers, and lower pumping rates. In the present study, we hypothesized that the structural differences in sponge anatomy influence their function, particularly the effect of spicules on the sponge pumping, and found that the inorganic spicule contents by their weight as well as volume form a major component of tissue density and sponge volume. Higher proportions of spicules were associated with reduced aquiferous structures and a lower pumping rate. Additionally, the inverse relationship of the proportion of the ash mass% and the AFDW in the sponge dry weight showed separate and distinct associations with aquiferous system variables such as porosity and the number of choanocytes per chamber. Wider surveys of proportions of the structural components in different-sized individuals of both HMA and LMA sponges will be useful for a greater understanding of the pumping physiology of sponges.

DATA AVAILABILITY STATEMENT

The original contributions presented in the study are included in the article/supplementary materials, further inquiries can be directed to the corresponding author.

AUTHOR CONTRIBUTIONS

All authors listed have made a substantial, direct and intellectual contribution to the work, and approved it for publication.

FUNDING

This work was supported by CSIR funded project Ocean Finder (PSC0105) and has NIO contribution no. 6817.

ACKNOWLEDGMENTS

We are grateful to The Director of National Institute of Oceanography, Council of Scientific and Industrial Research (CSIR) and The Academy of Scientific & Innovative Research (AcSIR), for the support and encouragement. We wish to express our appreciation to the editor and reviewers for their insightful comments. AD gratefully acknowledges University Grants Commission, India, for the award of Research Fellowship (UGC).

REFERENCES

Abercrombie, M. (1946). Estimation of nuclear population from microtome sections. *Anat. Rec.* 94, 239–247. doi: 10.1002/ar.1090940210

Alexander, B. E., Liebrand, K., Osinga, R., van der Geest, H. G., Admiraal, W., Cleutjens, J. P., et al. (2014). Cell turnover and detritus production in marine sponges from tropical and temperate benthic ecosystems. *PLoS ONE* 9:e109486. doi: 10.1371/journal.pone.0109486

Bell, J., Barnes, D., and Turner, J. (2002). The importance of micro and macro morphological variation in the adaptation of a sublittoral demosponge to current extremes. *Mar. Biol.* 140, 75–81. doi: 10.1007/s00227010 0665

Bergquist, P. R. (1978). *Sponges*. Berkeley, CA: University of California Press.

Chanas, B., and Pawlik, J. R. (1995). Defenses of Caribbean sponges against predatory reef fish. II. Spicules, tissue toughness, and nutritional quality. *Mar. Ecol. Progr. Series* 127, 195–211. doi: 10.3354/meps127195

De Goeij, J. M., De Kluijver, A., Van Duyl, F. C., Vacelet, J., Wijffels, R. H., De Goeij, A. F. P. M., et al. (2009). Cell kinetics of the marine sponge Halisarca caerulea reveal rapid cell turnover and shedding. *J. Exp. Biol.* 212, 3892–3900. doi: 10.1242/jeb.034561

De Goeij, J. M., Van Oevelen, D., Vermeij, M. J., Osinga, R., Middelburg, J. J., De Goeij, A. F., et al. (2013). Surviving in a marine desert: the sponge loop retains resources within coral reefs. *Science* 342, 108–110. doi: 10.1126/science.1241981

de Weerdt, W. H. (1986). A systematic revision of the north-eastern Atlantic shallow-water Haplosclerida (Porifera, Demospongiae): 2 Chalinidae. *Beaufortia* 36, 81–165.

Elliott, G. R., and Leys, S. P. (2007). Coordinated contractions effectively expel water from the aquiferous system of a freshwater sponge. *J. Exp. Biol.* 210, 3736–3748. doi: 10.1242/jeb.003392

Ellwanger, K., and Nickel, M. (2006). Neuroactive substances specifically modulate rhythmic body contractions in the nerveless metazoonTethyawilhelma (Demospongiae, Porifera). *Front. Zool.* 3:7. doi: 10.1186/1742-9994-3-7

Elvin, D. W. (1976). Seasonal growth and reproduction of an intertidal sponge, Haliclona permollis (Bowerbank). *Biol. Bull.* 151, 108–125. doi: 10.2307/1540709

Ereskovskii, A. V. (2003). Problems of coloniality, modularity, and individuality in sponges and special features of their morphogeneses during growth and asexual reproduction. *Rus. J. Mar. Biol.* 29, S46–S56. doi: 10.1023/B:RUMB.0000011716.90730.ac

Ereskovsky, A. V. (2000). Reproduction cycles and strategies of the cold-water sponges Halisarca dujardini (Demospongiae, Halisarcida), Myxilla incrustans and Iophon piceus (Demospongiae, Poecilosclerida) from the White Sea. *Biol. Bull.* 198, 77–87. doi: 10.2307/1542805

Ereskovsky, A. V., and Gonobobleva, E. L. (2000). New data on embryonic development of Halisarca dujardini Johnston, 1842 (Demospongiae, Halisarcida). *Zoosystema* 22, 355–368.

Erpenbeck, D., Sutcliffe, P., Cook, S. D. C., Dietzel, A., Maldonado, M., van Soest, R. W., et al. (2012). Horny sponges and their affairs: On the phylogenetic relationships of keratose sponges. *Mol. Phylogen. Evol.* 63, 809–816. doi: 10.1016/j.ympev.2012.02.024

Erwin, P. M., Coma, R., López-Sendino, P., Serrano, E., and Ribes, M. (2015). Stable symbionts across the HMA-LMA dichotomy: low seasonal and interannual variation in sponge-associated bacteria from taxonomically diverse hosts. *FEMS Microbiol. Ecol.* 91. doi: 10.1093/femsec/fiv115

Fang, J. K., Schönberg, C. H., Kline, D. I., Hoegh-Guldberg, O., and Dove, S. (2013). Methods to quantify components of the excavating sponge Cliona orientalis Thiele, 1900. *Mar. Ecol.* 34, 193–206. doi: 10.1111/maec.12005

Fry, W. G. (1979). "Taxonomy, the individual and the sponge," in *Biology and systematics of colonial organisms*. Systematics Association, Vol. 11 eds G. Larwood and B. R. Rosen (London: Academic Press), 39–80.

Fry, W. G. (ed.) (1970). "The sponge as a population: a biometric approach," in The Biology of Porifera. *Symposia of the Zoological Society of London*, Vol. 25 (London: Academic Press), 135–162.

Funayama, N., Nakatsukasa, M., Hayashi, T., and Agata, K. (2005). Isolation of the choanocyte in the fresh water sponge, Ephydatiafluviatilis and its lineage marker, Ef annexin. *Dev. Growth Diff.* 47, 243–253. doi: 10.1111/j.1440-169X.2005.00800.x

Gerasimova, E. I., and Ereskovsky, A. V. (2007). Reproduction of two species of Halichondria (Demospongiae: Halichondriidae) in the White Sea. Porifera Research-Biodiversity, innovation and sustainability. *Série Livros* 28, 327–333.

Gili J M Coma, R. (1998). Benthic suspension feeders: their paramount role in littoral marine food webs. *Trends Ecol. Evol.* 13, 316–321. doi: 10.1016/S0169-5347(98)01365-2

Gloeckner, V., Wehrl, M., Moitinho-Silva, L., Gernert, C., Schupp, P., Pawlik, J. R., et al. (2014). The HMA-LMA dichotomy revisited: an electron microscopical survey of 56 sponge species. *Biol. Bullet.* 227, 78–88. doi: 10.1086/BBLv227n1p78

Goldstein, J., Bisbo, N., Funch, P., and Riisgård, H. U. (2020). Contraction-expansion and the effects on the aquiferous system in the demosponge Halichondria panicea. *Front. Mar. Sci*. 7:113. doi: 10.3389/fmars.2020.00113

Goldstein, J., Riisgård, H. U., and Larsen, P. S. (2019). Exhalant jet speed of single-osculum explants of the demosponge Halichondria panicea and basic properties of the sponge-pump. *J. Exp. Mar. Biol. Ecol.* 511, 82–90. doi: 10.1016/j.jembe.2018.11.009

Hadas, E., Ilan, M., and Shpigel, M. (2008). Oxygen consumption by a coral reef sponge. *J. Exp. Biol*. 211, 2185–2190. doi: 10.1242/jeb.015420

Hammel, J. U., Filatov, M. V., Herzen, J., Beckmann, F., Kaandorp, J. A., and Nickel, M. (2012). The non-hierarchical, non-uniformly branching topology of a leuconoid sponge aquiferous system revealed by 3D reconstruction and morphometrics using corrosion casting and X-ray microtomography. *Acta Zoologica* 93, 160–170. doi: 10.1111/j.1463-6395.2010.00492.x

Hammel, J. U., Herzen, J., Beckmann, F., and Nickel, M. (2009). Sponge budding is a spatiotemporal morphological patterning process: insights from synchrotron radiation-based x-ray microtomography into the asexual reproduction of Tethya wilhelma. *Front. Zool*. 6, 1–14. doi: 10.1186/1742-9994-6-19

Hammel, J. U., and Nickel, M. (2014). A new flow-regulating cell type in the demosponge Tethyawilhelma–functional cellular anatomy of a leuconoid canal system. *PLoS ONE* 9:e113153. doi: 10.1371/journal.pone.0113153

Hentsshel, U., Fieseler, L., Wehrl, M., Gernert C Steinert, M., Hacker, J., and Horn, M. (2003). "Microbial diversity of marine sponges," in *Molecular Marine Biology of Sponges,* ed W. E. G. Muller (Heidelberg: Springer Verlag), 60–88. doi: 10.1007/978-3-642-55519-0_3

Hollister, S. J. (2005). Porous scaffold design for tissue engineering. *Nat. Mater.* 4:518. doi: 10.1038/nmat1421

Hollister, S. J., Levy, R. A., Chu, T. M., Halloran, J. W., and Feinberg, S. E. (2000). An image-based approach for designing and manufacturing craniofacial scaffolds. *Int. J. Oral Maxillofac. Surg.* 29, 67–71. doi: 10.1034/j.1399-0020.2000.290115.x

Hutmacher, D. W. (2000). Scaffolds in tissue engineering bone and cartilage. *Biomaterials* 21, 2529–2543. doi: 10.1016/S0142-9612(00)00121-6

Ilan, M., and Abelson, A. (1995). The life of a sponge in a sandy lagoon. *Biol. Bullet.* 189, 363–369. doi: 10.2307/1542154

Kaandorp, J. A. (1991). Modelling growth forms of the sponge *Haliclonaoculata* (Porifera, Demospongiae) using fractal techniques. *Mar. Biol.* 110, 203–215. doi: 10.1007/BF01313706

Kumala, L., Riisgård, H. U., and Canfield, D. E. (2017). Osculum dynamics and filtration activity in small single-osculum explants of the demosponge *Halichondriapanicea*. *Mar. Ecol. Progr. Series* 572, 117–128. doi: 10.3354/meps12155

LaBarbera, M. (1990). Principles of design of fluid transport systems in zoology. *Science* 249, 992–1000. doi: 10.1126/science.2396104

Labarbera, M. (1995). "The design of fluid transport systems: a comparative perspective," in Flow-Dependent Regulation of Vascular Function, eds J. A. BevanGabor and K. M. Rubanyi (New York, NY: Springer), 3–27. doi: 10.1007/978-1-4614-7527-9_1

LaBarbera, M., and Vogel, S. (1982). The design of fluid transport systems in organisms: despite their apparent diversity, fluid transport systems display a fundamental unity of organization resulting from the constraints of a few design principles on natural selection. *Am. Sci.* 70, 54–60.

Langenbruch, P. F., and Jones, W. C. (1990). Body structure of marine sponges. VI. Choanocyte chamber structure in the Haplosclerida (Porifera, Demospongiae) and its relevance to the phylogenesis of the group. *J. Morphol.* 204, 1–8. doi: 10.1002/jmor.1052040102

Lawrence, M., and Jiang, Y. (2017). "Porosity, pore size distribution, micro-structure," in *Bio-aggregates Based Building Materials* (Dordrecht: Springer), 39–71. doi: 10.1007/978-94-024-1031-0_2

Leys, S. P., and Hill, A. (2012). The physiology and molecular biology of sponge tissues. *Adv. Mar. Biol.* 62, 1–56. doi: 10.1016/B978-0-12-394283-8.00001-1

Leys, S. P., Kahn, A. S., Fang, J. K. H., Kutti, T., and Bannister, R. J. (2018). Phagocytosis of microbial symbionts balances the carbon and nitrogen budget for the deep-water boreal sponge Geodiabarretti. *Limnol. Oceanogr.* 63, 187–202. doi: 10.1002/lno.10623

Leys, S. P., Yahel, G., Reidenbach, M. A., Tunnicliffe, V., Shavit, U., and Reiswig, H. M. (2011). The sponge pump: the role of current induced flow in the design of the sponge body plan. *PLoS ONE* 6:e27787. doi: 10.1371/journal.pone.0027787

Ludeman, D. A., Farrar, N., Riesgo, A., Paps, J., and Leys, S. P. (2014). Evolutionary origins of sensation in metazoans: functional evidence for a new sensory organ in sponges. *BMC Evolut. Biol.* 14:3. doi: 10.1186/1471-2148-14-3

Ludeman, D. A., Reidenbach, M. A., and Leys, S. P. (2016). The energetic cost of filtration by demosponges and their behavioural response to ambient currents. *J. Exp. Biol*. 220(Pt 6), 995–1007. doi: 10.1242/jeb.146076

Luter, H. M., Whalan, S., and Webster, N. S. (2012). The marine sponge *Ianthella basta* can recover from stress-induced tissue regression. *Hydrobiologia* 687, 227–235. doi: 10.1007/s10750-011-0887-x

Maldonado, M. (2009). Embryonic development of verongid demosponges supports the independent acquisition of spongin skeletons as an alternative to the siliceous skeleton of sponges. *Biol. J. Linn. Soc.* 97, 427–447. doi: 10.1111/j.1095-8312.2009.01202.x

Maldonado, M., Ribes, M., and van Duyl, F. C. (2012). Nutrient fluxes through sponges: biology, budgets, and ecological implications. *Adv. Marine Biol.* 62, 113–182. doi: 10.1016/B978-0-12-394283-8.00003-5

Massaro, A. J., Weisz, J. B., Hill, M. S., and Webster, N. S. (2012). Behavioral and morphological changes caused by thermal stress in the Great Barrier Reef sponge Rhopaloeidesodorabile. *J. Exp. Mar. Biol. Ecol.* 416, 55–60. doi: 10.1016/j.jembe.2012.02.008

McMurray, S. E., Johnson, Z. I., Hunt, D. E., Pawlik, J. R., and andFinelli, C. M. (2016). Selective feeding by the giant barrel sponge enhances foraging efficiency. *Limnol. Oceanogr.* 61, 1271–1286. doi: 10.1002/lno.10287

McMurray, S. E., Pawlik, J. R., and Finelli, C. M. (2014). Trait-mediated ecosystem impacts: how morphology and size affect pumping rates of the Caribbean giant barrel sponge. *Aquat. Biol.* 23, 1–13. doi: 10.3354/ab00612

McMurray, S. E., Stubler, A. D., Erwin, P. M., Finelli, C. M., and andPawlik, J. R. (2018). A test of the sponge-loop hypothesis for emergent Caribbean reef sponges. *Mar. Ecol. Progr.* 588, 1–14. doi: 10.3354/meps12466

Miron-Mendoza, M., Seemann, J., and Grinnell, F. (2010). The differential regulation of cell motile activity through matrix stiffness and porosity in three dimensional collagen matrices. *Biomaterials* 31, 6425–6435. doi: 10.1016/j.biomaterials.2010.04.064

Moitinho-Silva, L., Steinert, G., Nielsen, S., Hardoim, C., Wu, Y. C., McCormack, G. P., et al. (2017). Predicting the HMA-LMA status in marine sponges by machine learning. *Front. Microbiol.* 8:752. doi: 10.3389/fmicb.2017.00752

Morganti, T. M., Ribes, M., Moskovich, R., Weisz, J. B., Yahel, G., and Coma, R. (2021). *In situ* pumping rate of 20 marine demosponges is a function of osculum area. *Front. Mar. Sci.* 8:583188. doi: 10.3389/fmars.2021.712856

Morganti, T. M., Ribes, M., Yahel, G., and Coma, R. (2019). Size is the major determinant of pumping rates in marine sponges. *Front. Physiol.* 10:1474. doi: 10.3389/fphys.2019.01474

Nakayama, S., Arima, K., Kawai, K., Mohri, K., Inui, C., Sugano, W., et al. (2015). Dynamic transport and cementation of skeletal elements build up the pole-and-beam structured skeleton of sponges. *Curr. Biol.* 25, 2549–2554. doi: 10.1016/j.cub.2015.08.023

Nickel, M. (2004). Kinetics and rhythm of body contractions in the sponge Tethyawilhelma (Porifera: Demospongiae). *J. Exp. Biol.* 207, 4515–4524. doi: 10.1242/jeb.01289

Nickel, M. (2010). Evolutionary emergence of synaptic nervous systems: what can we learn from the non-synaptic, nerveless Porifera?. *Invertebr. Biol.* 129, 1–16. doi: 10.1111/j.1744-7410.2010.00193.x

Palumbi, S. R. (1984). Tactics of acclimation: morphological changes of sponges in an unpredictable environment. *Science* 225, 1478–1480. doi: 10.1126/science.225.4669.1478

Palumbi, S. R. (1986). How body plans limit acclimation: responses of a demosponge to wave force. *Ecology* 67, 208–214. doi: 10.2307/1938520

Pawlik, J. R., and McMurray, S. E. (2020). The emerging ecological and biogeochemical importance of sponges on coral reefs. *Ann. Rev. Mar. Sci.* 12, 315–337. doi: 10.1146/annurev-marine-010419-010807

Poppell, E., Weisz, J., Spicer, L., Massaro, A., Hill, A., and Hill, M. (2014). Sponge heterotrophic capacity and bacterial community structure in high-and low-microbial abundance sponges. *Mar. Ecol.* 35, 414–424. doi: 10.1111/maec.12098

Reiswig, H. M. (1971). *In situ* pumping activities of tropical Demospongiae. *Mar. Biol.* 9, 38–50. doi: 10.1007/BF00348816

Reiswig, H. M. (1975). Bacteria as food for temperate-water marine sponges. *Canad. J. Zool.* 53, 582–589. doi: 10.1139/z75-072

Reiswig, H. M. (1981). Partial carbon and energy budgets of the bacteriosponge *Verohgiafistularis* (Porifera: Demospongiae) in Barbados. *Mar. Ecol.* 2, 273–293. doi: 10.1111/j.1439-0485.1981.tb00271.x

Riisgård, H. U., Kumala, L., and Charitonidou, K. (2016). Using the F/R-ratio for an evaluation of the ability of the demosponge Halichondria panicea to nourish solely on phytoplankton versus free-living bacteria in the sea. *Mar. Biol. Res.* 12, 907–916. doi: 10.1080/17451000.2016.1206941

Riisgård, H. U., Thomassen, S., Jakobsen, H., Weeks, J. M., and Larsen, P. S. (1993). Suspension feeding in marine sponges *Halichondriapanicea* and *Haliclonaurceolus*: effects of temperature on filtration rate and energy cost of pumping. *Mar. Ecol. Progr. Series* 96, 177–188. doi: 10.3354/meps096177

Riisgaard, H. U., and Larsen, P. S. (1995). Filter-feeding in marine macro-invertebrates: pump characteristics, modelling and energy cost. *Biol. Rev.* 70, 67–106. doi: 10.1111/j.1469-185X.1995.tb01440.x

Sandford, F. (2003). Physical and chemical analysis of the siliceous skeletons in six sponges of two groups (Demospongiae and Hexactinellida). *Microsc. Res. Tech.* 62, 336–355. doi: 10.1002/jemt.10400

Schmitt, S., Weisz, J. B., Lindquist, N., and Hentschel, U. (2007). Vertical transmission of a phylogenetically complex microbial consortium in the viviparous sponge Ircinia felix. *Appl. Environ. Microbiol.* 73, 2067–2078. doi: 10.1128/AEM.01944-06

Schönberg, C. H. L. (2016). Happy relationships between marine sponges and sediments–a review and some observations from Australia. *J. Mar. Biol. Assoc. United Kingdom* 96, 493–514. doi: 10.1017/S0025315415001411

Shore, R. E. (1971). Growth and renewal studies of the choanocyte population in Hymeniacidon sinapium (Porifera: Demospongiae) using colcemid and 3H thymidine. *J. Exp. Zool.* 177, 359–363. doi: 10.1002/jez.1401770310

Sim, C. J., and Lee, K. J. (2002). Two new psammocinian sponges (Dictyoceratida: Irciniidae) from Korea. *Kor. J. Biol. Sci.* 6, 53–57. doi: 10.1080/12265071.2002.9647633

Simpson, T. L. (1984). *The Cell Biology of Sponges*. New York,NY: Springer-Verlag. doi: 10.1007/978-1-4612-5214-6

Strehlow, B. W., Jorgensen, D., Webster, N. S., Pineda, M. C., and Duckworth, A. (2016). Using a thermistor flowmeter with attached video camera for monitoring sponge excurrent speed and oscular behaviour. *PeerJ* 4:e2761. doi: 10.7717/peerj.2761

Szitenberg, A., Becking, L. E., Vargas, S., Fernandez, J. C., Santodomingo, N., Wörheide, G., et al. (2013). Phylogeny of Tetillidae (Porifera, Demospongiae, Spirophorida) based on three molecular markers. *Mol. Phylogenet. Evol.* 67, 509–519. doi: 10.1016/j.ympev.2013.02.018

Tanaka-Ichihara, K., and Watanabe, Y. (1990). "Gamatogenic cycle in Halichondria okadai," in *New Perspective in Sponge Biology*, ed K. Rutzler (Washington, DC: Simthsonian Institution Press), 170–174.

Taylor, M. W., Radax, R., Steger, D., and Wagner, M. (2007). Sponge-associated microorganisms: evolution, ecology, and biotechnological potential. *Microbiol. Mol. Biol. Rev.* 71, 295–347. doi: 10.1128/MMBR.00040-06

Tsurumi, M. A. I. A., and Reiswig, H. M. (1997). Sexual versus asexual reproduction in an oviparous rope-form sponge, Aplysina cauliformis (Porifera; Verongida). *Invertebrate Reprod. Dev.* 32, 1–9. doi: 10.1080/07924259.1997.9672598

Turon, M., Cáliz, J., Garate, L., Casamayor, E. O., and Uriz, M. J. (2018). Showcasing the role of seawater in bacteria recruitment and microbiome stability in sponges. *Sci. Rep.* 8, 1–10. doi: 10.1038/s41598-018-33545-1

Turon, X., Galera, J., and Uriz, M. J. (1997). Clearance rates and aquiferous systems in two sponges with contrasting life-history strategies. *J. Exp. Zool.* 278, 22–363. doi: 10.1002/(SICI)1097-010X(19970501)278:1<22::AID-JEZ3>3.0.CO;2-8

Uriz, M. J. (2006). Mineral skeletogenesis in sponges. *Canad. J. Zool.* 84, 322–356. doi: 10.1139/z06-032

Uriz, M. J., Turon, X., Becerro, M. A., and Agell, G. (2003). Siliceous spicules and skeleton frameworks in sponges: origin, diversity, ultrastructural patterns, and biological functions. *Microscopy Res. Tech.* 62, 279–299. doi: 10.1002/jemt.10395

Vacelet, J., Boury-Esnault, N., De Vos, L., and Donadey, C. (1989). Comparative study of the choanosome of Porifera: II. The keratose sponges. *J. Morphol.* 201, 119–129. doi: 10.1002/jmor.1052010203

Vacelet, J., and Donadey, C. (1977). Electron microscope study of the association between some sponges and bacteria. *J. Exp. Mar. Biol. Ecol.* 30, 301–314. doi: 10.1016/0022-0981(77)90038-7

Vogel, S. (1996). *Life in Moving Fluids: The Physical Biology of Flow-Revised and Expanded Second Edition*. Princeton University Press.

Watson, J. R., Krömer, J. O., Degnan, B. M., and Degnan, S. M. (2017). Seasonal changes in environmental nutrient availability and biomass composition in a coral reef sponge. *Mar. Biol.* 164, 135. doi: 10.1007/s00227-017-3167-0

Webster, N. S., Taylor, M. W., Behnam, F., Lücker, S., Rattei, T., Whalan, S., et al. (2010). Deep sequencing reveals exceptional diversity and modes of transmission for bacterial sponge symbionts. *Environ. Microbiol.* 12, 2070–2082. doi: 10.1111/j.1462-2920.2009.02065.x

Weisz, J. B., Lindquist, N., and Martens, C. S. (2008). Do associated microbial abundances impact marine demosponge pumping rates and tissue densities? *Oecologia* 155, 367–376. doi: 10.1007/s00442-007-0910-0

Werding, B., and Sanchez, H. (1991). Life habits and functional morphology of the sediment infaunal sponges *Oceanapia oleracea* and *Oceanapiapeltata* (Porifera, Haplosclerida). *Zoomorphology* 110, 203–208. doi: 10.1007/BF01633004

Wilkinson, C. R. (1978). Microbial associations in sponges. I. Ecology, physiology and microbial populations of coral reef sponges. *Mar. Biol.* 49, 161–167. doi: 10.1007/BF00387115

Wilkinson, C. R. (1983). Net primary productivity in coral reef sponges. *Science* 219, 410–412. doi: 10.1126/science.219.4583.410

Yahel, G., Sharp, J. H., Marie, D., and Häse2, C., andGenin, A. (2003). *In situ* feeding and element removal in the symbiont-bearing sponge Theonellaswinhoei: bulk DOC is the major source for carbon. *Limnol. Oceanogr.* 48, 141–149. doi: 10.4319/lo.2003.48.1.0141

Conflict of Interest: The authors declare that the research was conducted in the absence of any commercial or financial relationships that could be construed as a potential conflict of interest.

Publisher's Note: All claims expressed in this article are solely those of the authors and do not necessarily represent those of their affiliated organizations, or those of the publisher, the editors and the reviewers. Any product that may be evaluated in this article, or claim that may be made by its manufacturer, is not guaranteed or endorsed by the publisher.